Awake Hippocampal Sharp-Wave Ripples Support Spatial Memory

Shantanu P. Jadhav *et al.*

Science **336**, 1454 (2012);
DOI: 10.1126/science.1217230

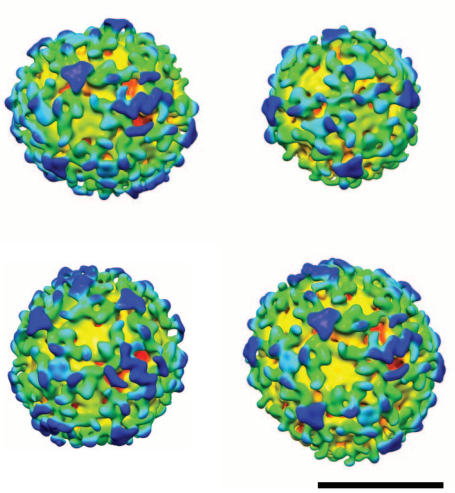

Fig. 4. The structures of COPI-coated vesicles. Isosurface representations of four COPI-coated vesicles produced by positioning reconstructions of triads and triad patterns (Figs. 2 and 3, K to N) at the positions and orientations in space at which they were identified during subtomogram averaging. Densities are colored as in Fig. 2. Scale bar, 50 nm.

found in each vesicle and were merged to create continuous density models of individual vesicles (Fig. 4 and movie S2). These models suggest that the COPI coat contains only small apertures (Fig. 4 and fig. S1). Sufficient membrane access for fusion with a target membrane could only be achieved after coat disassembly or through budding scars. In contrast, clathrin and COPII cages form lattices with larger apertures (fig. S1).

In existing models for clathrin and COPII vesicle coats, multiple identical subunits each make the same set of interactions with the same number of neighbors (*1*). Structural flexibility allows formation of vesicles from different total numbers of subunits. Based on these principles, both clathrin-like (*20*) and COPII-like (*23*) models have been proposed for the assembled COPI coat. We found instead that assembled coatomer can adopt different conformations to interact with different numbers of neighbors. By regulating the relative frequencies of different triad patterns in the COPI coat during assembly— for example, by stabilizing particular coatomer conformations— the cell would have a mechanism to adapt vesicle size and shape to cargoes of different sizes.

References and Notes

1. S. C. Harrison, T. Kirchhausen, *Nature* **466**, 1048 (2010).
2. H. T. McMahon, I. G. Mills, *Curr. Opin. Cell Biol.* **16**, 379 (2004).
3. K. Schledzewski, H. Brinkmann, R. R. Mendel, *J. Mol. Evol.* **48**, 770 (1999).
4. A. Fotin *et al.*, *Nature* **432**, 573 (2004).
5. S. M. Stagg *et al.*, *Nature* **439**, 234 (2006).
6. S. M. Stagg, P. LaPointe, W. E. Balch, *Curr. Opin. Struct. Biol.* **17**, 221 (2007).
7. Y. Cheng, W. Boll, T. Kirchhausen, S. C. Harrison, T. Walz, *J. Mol. Biol.* **365**, 892 (2007).
8. R. Beck, M. Rawet, F. T. Wieland, D. Cassel, *FEBS Lett.* **583**, 2701 (2009).
9. S. Hara-Kuge *et al.*, *J. Cell Biol.* **124**, 883 (1994).
10. C. K. Yip, T. Walz, *J. Mol. Biol.* **408**, 825 (2011).
11. M. C. Sahlmüller *et al.*, *Traffic* **12**, 682 (2011).
12. G. Griffiths, R. Pepperkok, J. K. Locker, T. E. Kreis, *J. Cell Sci.* **108**, 2839 (1995).
13. M. Bremser *et al.*, *Cell* **96**, 495 (1999).
14. L. Orci, B. S. Glick, J. E. Rothman, *Cell* **46**, 171 (1986).
15. J. A. Briggs *et al.*, *Proc. Natl. Acad. Sci. U.S.A.* **106**, 11090 (2009).
16. F. Förster, O. Medalia, N. Zauberman, W. Baumeister, D. Fass, *Proc. Natl. Acad. Sci. U.S.A.* **102**, 4729 (2005).
17. Materials and methods are available as supplementary materials on *Science* Online.
18. L. P. Jackson *et al.*, *Cell* **141**, 1220 (2010).
19. X. Yu, M. Breitman, J. Goldberg, *Cell* **148**, 530 (2012).
20. C. Lee, J. Goldberg, *Cell* **142**, 123 (2010).
21. D. K. Cureton, R. H. Massol, S. Saffarian, T. L. Kirchhausen, S. P. Whelan, *PLoS Pathog.* **5**, e1000394 (2009).
22. V. Sirotkin, J. Berro, K. Macmillan, L. Zhao, T. D. Pollard, *Mol. Biol. Cell* **21**, 2894 (2010).
23. K. C. Hsia, A. Hoelz, *Proc. Natl. Acad. Sci. U.S.A.* **107**, 11271 (2010).

Acknowledgments: We thank M. Beck, J. Ellenberg, M. Kaksonen, and S. Welsch for critically reading the manuscript and F. Thommen, T. Bharat, and A. de Marco for technical assistance. This work was funded by the Deutsche Forschungsgemeinschaft within SFB638 (A16) to J.A.G.B. and F.T.W., by Bundesministerium für Bildung und Forschung to K.B., and was technically supported by use of the European Molecular Biology Laboratory EM Core Facility and Information Technology Services. EM maps are deposited in the Electron Microscopy Data Bank (EMDB) (accession codes from EMD-2084 to EMD-2088). J.A.G.B. and F.T.W. conceived and administered the study. S.P., M.F., and R.B. reconstituted budding reactions, supported by K.B. and B.B. S.P., R.B., and K.B. prepared reagents. M.F., S.P., and J.D.R. collected data. M.F., M.S., and J.A.G.B. developed image processing routines. M.F. and J.A.G.B. analyzed data. M.F., F.T.W. and J.A.G.B. interpreted data. M.F. and J.A.G.B. wrote the paper, supported by all authors.

Supplementary Materials

www.sciencemag.org/cgi/content/full/science.1221443/DC1
Materials and Methods
Figs. S1 to S6
References (*24*–*31*)
Movies S1 and S2

5 March 2012; accepted 2 May 2012
Published online 24 May 2012;
10.1126/science.1221443

Awake Hippocampal Sharp-Wave Ripples Support Spatial Memory

Shantanu P. Jadhav, Caleb Kemere, P. Walter German, Loren M. Frank*

The hippocampus is critical for spatial learning and memory. Hippocampal neurons in awake animals exhibit place field activity that encodes current location, as well as sharp-wave ripple (SWR) activity during which representations based on past experiences are often replayed. The relationship between these patterns of activity and the memory functions of the hippocampus is poorly understood. We interrupted awake SWRs in animals learning a spatial alternation task. We observed a specific learning and performance deficit that persisted throughout training. This deficit was associated with awake SWR activity, as SWR interruption left place field activity and post-experience SWR reactivation intact. These results provide a link between awake SWRs and hippocampal memory processes, which suggests that awake replay of memory-related information during SWRs supports learning and memory-guided decision-making.

Animals use past experience to guide decisions, an ability that requires storing memories for the events of daily life and retrieving those memories as needed. This storage and retrieval depends on the hippocampus and associated structures in the medial temporal lobe (*1*–*5*), but the specific patterns of neural activity that support these memory functions remain poorly understood. We know that during exploration, individual neurons fire in specific regions of space (*5*, *6*) known as place fields. In contrast, during periods of slow movement, immobility, and slow-wave sleep, groups of neurons are active during sharp-wave ripple (SWR) events (*7*, *8*). This activity frequently represents a replay of a past experience on a rapid time scale (*9*–*13*). SWRs that occur during sleep contribute to memory consolidation of preceding experiences (*14*–*18*), and both changes in place fields and the intensity of awake memory reactivation have been correlated with memory performance (*19*). Awake SWRs in particular can reactivate sets of place fields encoding forward and reverse paths associated with both current and past locations (*9*–*13*). This reactivation has been hypothesized to contribute to multiple functions including learning, retrieval, consolidation, and trajectory planning (*19*–*23*). To investigate the role of awake hippocampal SWRs and to determine whether awake replay can be functionally dissociated from place field activity, we selectively disrupted awake SWRs in rats learning a hippocampus-dependent W-track task (*24*). We have previously shown that the hippocampus frequently replays memories of past experience while animals learn this task (*11*).

Animals are rewarded on the W-track each time they visit the end of one of the three maze arms in the correct task sequence (center-left-center-right-center…, Fig. 1A). This task consists

Department of Physiology and Center for Integrative Neuroscience, University of California, San Francisco, CA 94143, USA.

*To whom correspondence should be addressed. E-mail: loren@phy.ucsf.edu

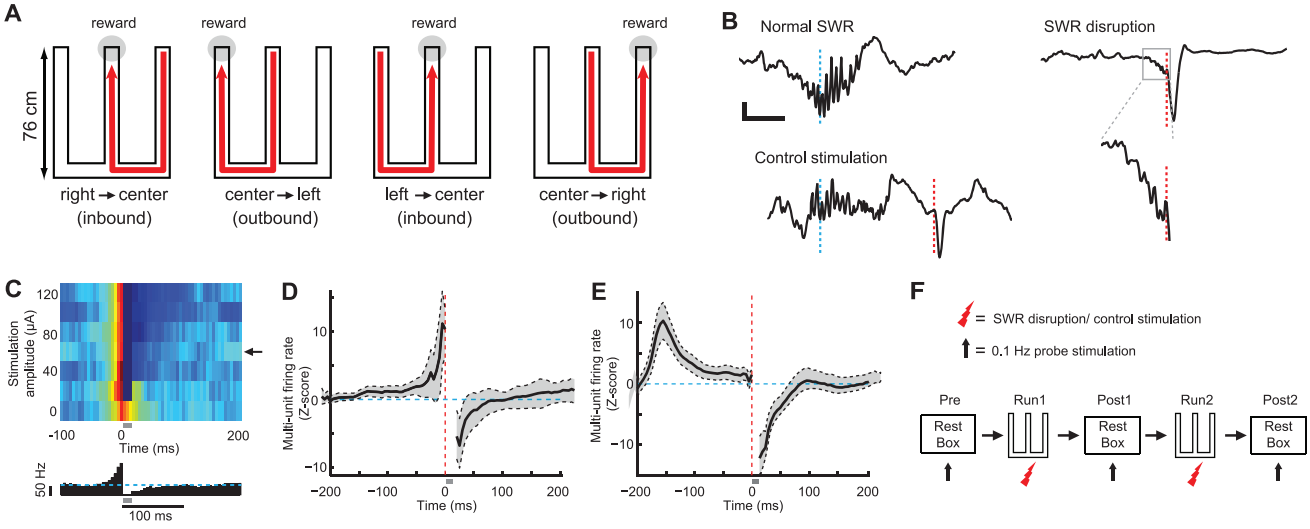

Fig. 1. Experimental design and SWR disruption during behavior. (**A**) Schematic illustrating the W-track task. (**B**) Example of a normal SWR (top left), disrupted SWR (right), and control stimulation after SWR (bottom left). Each panel shows an online detected SWR in the broadband local field potential (1 to 400 Hz). Cyan lines denote time of SWR detection; red lines denote time of vHC stimulation. The region in the gray box for the disrupted SWR is expanded below. Scale bars, 50 ms and 200 μV. (**C**) Top: Mean normalized multiunit activity (5-ms bins) versus stimulation intensity during calibration. Arrow denotes chosen amplitude. Bottom: Corresponding histogram for chosen amplitude; cyan line denotes baseline firing rate. Gray bar denotes spiking obscured by stimulation artifacts and fPSPs. (**D** and **E**) *Z* scores of multiunit firing rate aligned to stimulation for all sessions for the SWR disruption group (D) and the control stimulation group (E). Vertical red lines show the time of stimulation; horizontal cyan lines denote mean firing rates. (**F**) Sequence of rest and run sessions for each day.

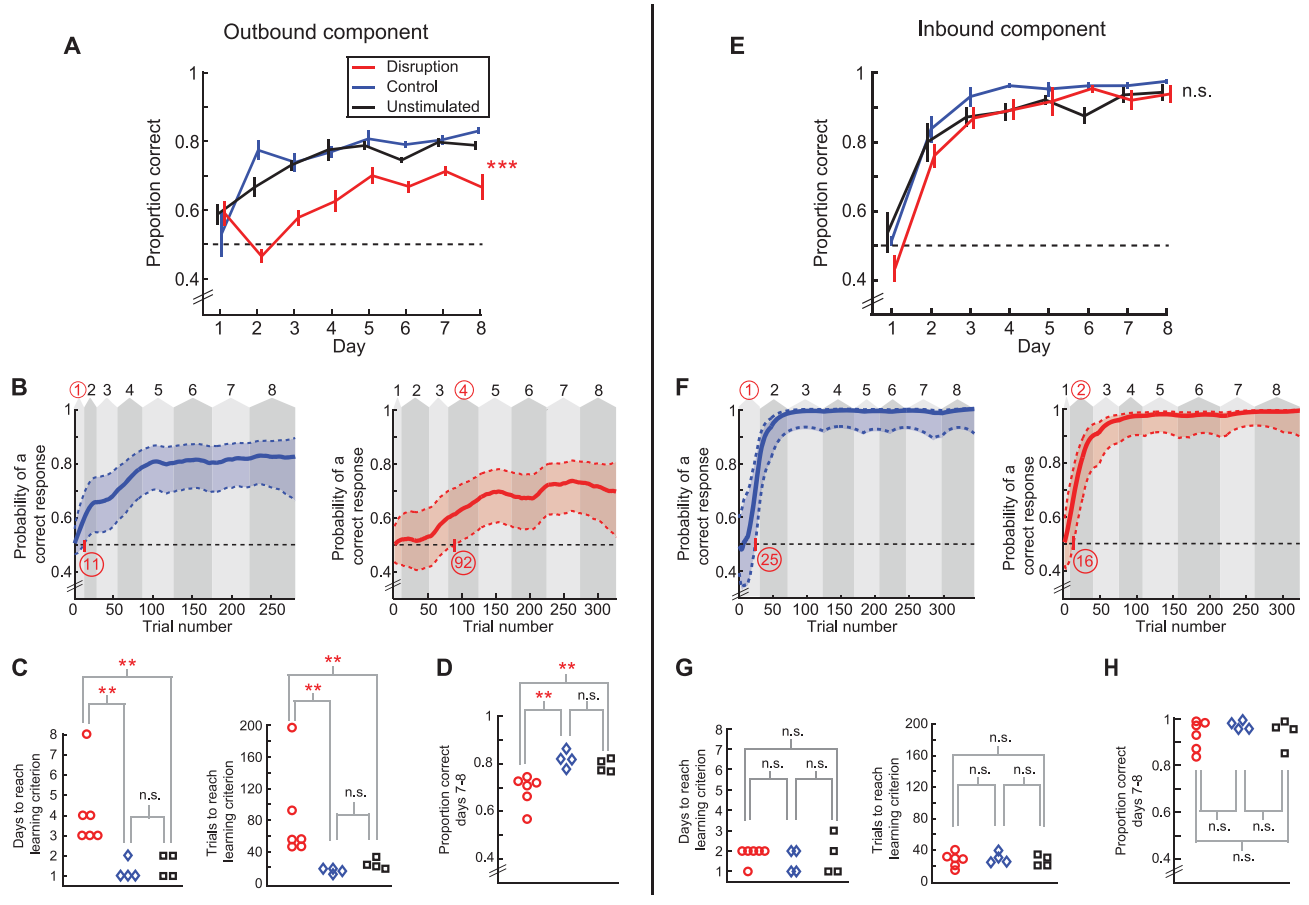

Fig. 2. SWR disruption causes a specific impairment in the outbound, spatial working memory component of the W-track task. (**A**) Proportion correct versus day number for outbound trials. Horizontal dotted line represents chance-level performance of 0.5. (**B**) Outbound learning curves with 90% confidence intervals for a control stimulation animal (left) and a SWR disruption animal (right). Background shaded areas denote days (numbers on top). Learning trial and learning day are highlighted in red. (**C**) Outbound learning day (left) and learning trial (right) for each animal. (**D**) Average outbound performance on the last 2 days of testing (days 7 and 8). (**E** to **H**) Corresponding plots for inbound performance. *P < 0.05, **P < 0.01, ***P < 0.001; error bars represent SEM.

of two components: (i) an "outbound" alternation component that specifies that when the animal is in the center arm, the next correct outer arm is the one opposite to the outer arm it most recently visited, and (ii) an "inbound" return-to-center component that specifies that when the animal is in an outer arm, it must then proceed to the center arm. Hippocampal damage impairs the rapid learning of both components, although hippocampal-lesion animals eventually learn the task (*24*), which suggests that other structures such as the basal ganglia and prefrontal cortex can support task performance after extended training.

We disrupted awake hippocampal SWRs on the W-track across 8 days of learning with the use of an online feedback system similar to that used in previous studies that disrupted SWRs during post-behavior sleep (*17*, *18*). SWRs in CA1 were detected by monitoring power in the ripple band (*25*) simultaneously across multiple tetrodes. Online detection of a SWR event triggered calibrated single-pulse electrical stimulation of CA3 afferents to CA1 delivered through a bipolar stimulation electrode in the ventral hippocampal commissure (vHC, fig. S1). This terminated the ripple oscillation within 25 ms of SWR onset and transiently inhibited CA1 spiking (Fig. 1, B to E, and fig. S2) (*25*). We calibrated the stimulation magnitude for each animal to find the minimum current that inhibited multiunit spiking activity in CA1 for ~100 ms (Fig. 1, C to E, and fig. S2). To ensure that any observed effects were due to disruption of activity during SWRs, we used the same online detection protocol in a control group of animals, but delayed stimulation by 150 to 200 ms after detection (*17*) (Fig. 1, B and E, and fig. S2). This control stimulation left SWR-associated spiking activity intact while still inhibiting a temporally equivalent period of hippocampal activity (Fig. 1E).

Animals in three groups—SWR disruption, control stimulation, and an unimplanted, unstimulated group (n = 6, 4, and 4, respectively)—ran

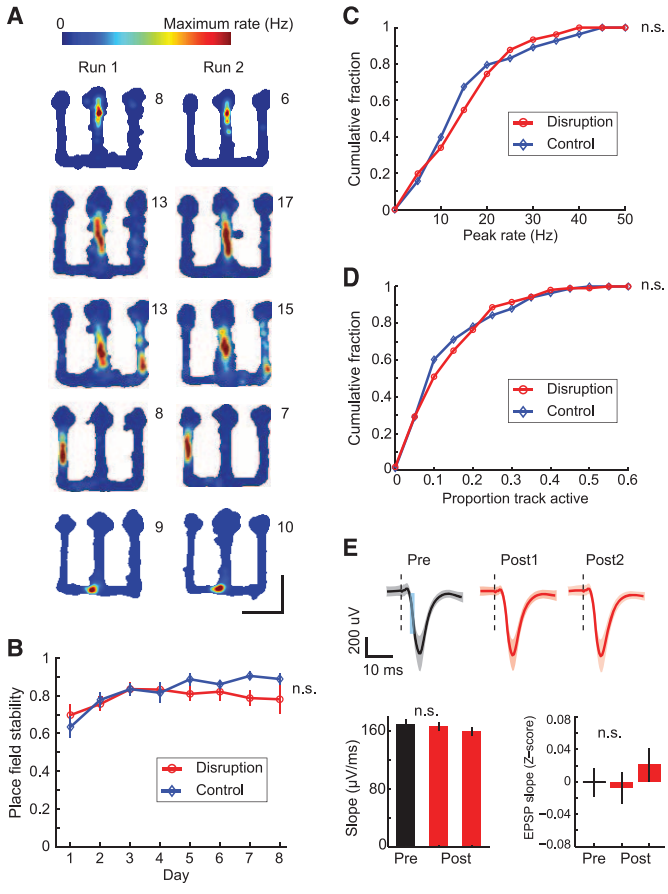

Fig. 3. Intact place-field representations and unchanged PSPs in SWR disruption animals. (**A**) Place fields from SWR disruption animals across run sessions within a day. Color plots represent occupancy-normalized firing rates of place cells. Numbers on top right of each plot denote peak spatial firing rate. Cells are from days 2, 3, 4, 6, and 8 (top to bottom), respectively. (**B**) Place field stability across days. (**C**) Cumulative distribution function (CDF) of place field peak rates. (**D**) CDF of place field sizes. (**E**) Evoked field responses during rest sessions. Top: Example showing mean evoked field PSPs during rest sessions in a single day in a SWR disruption animal. Shaded areas represent SEM. Dotted black lines indicate time of stimulation. Slopes of field PSPs were measured in the 1.5- to 2-ms window illustrated by cyan area in the left panel. Bottom: Slopes for the example above (left), and Z scores of field PSP slopes in the pre and post rest sessions for the SWR disruption group (right).

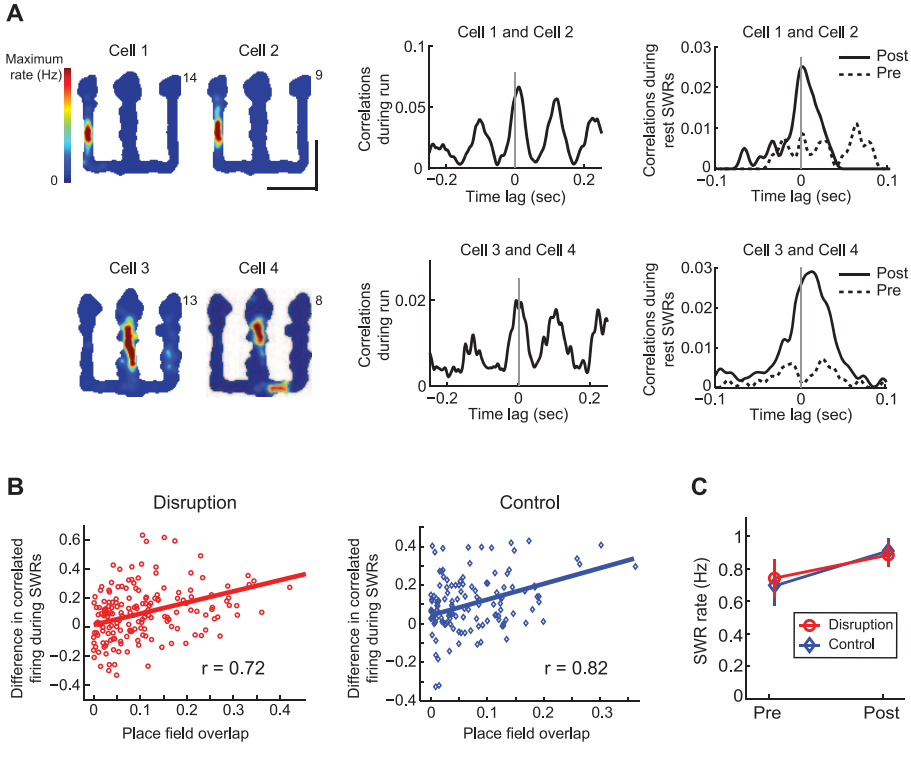

Fig. 4. Reactivation during SWRs in rest periods after behavior is intact. (**A**) Examples of reactivation from SWR disruption animals. Left: Place fields for cells during run sessions. Center: Cross-correlations for the cell pairs during run. Right: Cross-correlations during SWRs in rest periods. (**B**) Reactivation strength versus place field overlap for all cell pairs in the two groups (n = 183 pairs for the SWR disruption group; n = 145 pairs for the control stimulation group). Line represents best linear fit corresponding to the r value. (**C**) Mean SWR rate during the pre and post rest sessions. Error bars represent SEM.

two 15-min sessions on the W-track with interleaving 15-min rest sessions (one "pre" rest session before behavior and two "post" rest sessions after behavior) each day (Fig. 1F) for a total of 8 days. Spiking activity in CA1 was monitored during all run and rest sessions in the SWR disruption and control stimulation groups. To control for the possibility that vHC stimulation could lead to changes in the synaptic strength of CA3 input to CA1, we also measured evoked field responses to 0.1-Hz probe stimulation in the intervening rest periods (Fig. 1F) (*25*).

SWR disruption animals were impaired on the outbound component of the task as compared to controls (Fig. 2, A to D). SWR disruption animals performed a lower proportion of correct outbound trials than the control animals across all eight days of learning (Fig. 2A; n = 6, 4, and 4 animals, repeated-measures ANOVA, main effect of group, $P < 0.001$, group × day interaction, $P < 0.01$; no differences between control and unstimulated group, Ps > 0.4). We also used a state-space model to estimate the trial and day on which performance was above chance for each animal (*24*–*26*) (Fig. 2B and figs. S3 to S5). SWR disruption animals learned later than controls in terms of both trials and days to criterion (Fig. 2C, rank-sum test, Ps < 0.01). SWR disruption animals also had significantly lower performance levels on the final 2 days (Fig. 2D, rank-sum test, $P < 0.01$). Further, all SWR disruption animals learned more slowly than all eight control animals, and all SWR disruption animals had lower performance on days 7 and 8 than all eight control animals. These perfect separations in the rank order of learning rates and final performance would occur by chance with a probability < 0.0007. Similar statistical results were obtained with the two control groups combined (*25*).

In contrast, SWR disruption animals performed normally in the inbound component of the task (Fig. 2E; n = 6, 4, and 4 animals, repeated-measures ANOVA, main effect of group, $P > 0.33$, group × day interaction, $P > 0.5$) and had similar learning rates as compared to controls (Fig. 2F and figs. S6 to S8). Learning trial and day were similar among the SWR disruption and control groups (Fig. 2G, rank-sum tests, Ps > 0.5), and the final performance levels achieved by the animals in the last 2 days were also similar (Fig. 2H, rank-sum test, $P > 0.48$). The distinction between learning on the outbound and inbound tasks remained clear when learning curves were aligned by trial number for the three groups (fig. S9).

SWR disruption effectively suppressed hippocampal activity during SWRs but had no discernible effect on place cell representations. We examined the stability of CA1 place fields in run sessions (Fig. 3A and fig. S10) and computed the correlation between linearized place fields (*11*, *25*, *27*) of each cell across the two run sessions within each day (Fig. 3, A and B, and fig. S11). We found no difference in place field stability between place cells from the two groups (SWR disruption: n = 108 place cells, mean correlation = 0.80 ± 0.02; control stimulation: n = 96 cells, mean correlation = 0.81 ± 0.02; t test, $P > 0.5$) across all days (Fig. 3B; two-way ANOVA, main effect of group, $P > 0.16$, group × day interaction, $P > 0.5$; within-day comparisons, n.s.; Bonferroni post hoc tests). The distributions of peak rates and place field sizes for the two groups were also similar (Fig. 3, C and D; KS test, Ps > 0.5). We also found no evidence that stimulation induced synaptic plasticity. We found no difference in field postsynaptic potential (PSP) slopes in response to 0.1-Hz probe stimulation between the pre rest period before behavior and the post rest periods after behavior compared on each day for all animals (example and Z scores across all days in Fig. 3E, n.s., t test, $P > 0.43$). Further, differences in other behavior or stimulation parameters could not account for the learning deficit in the SWR disruption group. (figs. S12 to S17).

The deficit on outbound but not inbound trials suggests that loss of awake SWRs did not cause a global deficit in memory consolidation. Consistent with this, we found no evidence for alteration of the rest/sleep SWR activity associated with consolidation. Pairs of cells with overlapping place fields had theta-modulated correlations during run periods and showed increased correlations during SWRs in post relative to pre rest periods (Fig. 4A), as has been observed in animals with intact hippocampal activity (*14*, *16*, *28*). For both SWR disruption and control stimulation groups, reactivation strength (Fig. 4B) was significantly correlated with place field overlap (linear regression, Ps < 0.001) and with correlations during run (fig. S18; linear regression, Ps < 0.001). SWR rates in the rest periods were also similar for the SWR disruption and control stimulation groups (Fig. 4C and fig. S18).

Our observation of intact place fields, intact reactivation during rest SWRs, and intact inbound performance suggests that place fields and post-experience reactivation are sufficient to support learning and performance of the inbound trials. As hippocampal lesions disrupt learning on the inbound component, place cell activity may be important for learning and applying the inbound rule. More broadly, place cell activity could provide information about current position that promotes rapid learning and application of location-specific rules (fig. S19).

The specific performance deficit observed in SWR disruption animals provides a causal link between awake hippocampal SWRs and the spatial memory requirements of outbound trials. Learning of the outbound rule requires linking immediate and more remote past experience to reward (fig. S19), and the observed replay of both recent and remote experiences during awake SWRs (*11*–*13*) is well suited to contribute to this learning. Applying the outbound rule in the center arm requires knowledge of current location, memory for immediate past outer arm location, and the ability to use that memory to plan and execute a movement to the opposite outer arm. This memory-guided decision-making process has been referred to as "spatial working memory" (*2*, *4*). Impaired outbound performance in the SWR disruption group on later days (Fig. 2), even after most animals performed above chance, suggests a spatial working memory impairment. Additional evidence for this was provided by a decline in performance in three of the animals from the control stimulation group that were switched to SWR disruption on days 9 and 10 (fig. S20). Forward and backward replay of both past and possible future trajectories during SWRs (*9*–*13*, *21*) may therefore contribute to outbound performance. Conversely, we would predict that manipulations that cause selective spatial working memory deficits, such as the removal of parvalbumin-positive interneurons in CA1 and GluR1 knockout animals at the CA3-CA1 synapse (*29*, *30*), have their impact primarily as a result of disrupting awake replay processes. Thus, we hypothesize that the forward and reverse replay of local and spatially remote paths seen during awake replay provides information about past locations and possible future options (fig. S19) to structures such as the prefrontal cortex that use this information to learn the outbound alternation rule and to subsequently apply the learned rule to guide behavior.

References and Notes

1. L. R. Squire, *Psychol. Rev.* **99**, 195 (1992).
2. H. Eichenbaum, N. J. Cohen, *From Conditioning to Conscious Recollection* (Oxford Univ. Press, New York, 2001).
3. G. Riedel *et al*., *Nat. Neurosci.* **2**, 898 (1999).
4. D. S. Olton, J. T. Becker, G. E. Handelmann, *Behav. Brain Sci.* **2**, 313 (1979).
5. J. O'Keefe, L. Nadel, *The Hippocampus as a Cognitive Map* (Oxford Univ. Press, London, 1978).
6. M. A. Wilson, B. L. McNaughton, *Science* **261**, 1055 (1993).
7. G. Buzsáki, *Brain Res.* **398**, 242 (1986).
8. J. O'Neill, T. Senior, J. Csicsvari, *Neuron* **49**, 143 (2006).
9. D. J. Foster, M. A. Wilson, *Nature* **440**, 680 (2006).
10. K. Diba, G. Buzsáki, *Nat. Neurosci.* **10**, 1241 (2007).
11. M. P. Karlsson, L. M. Frank, *Nat. Neurosci.* **12**, 913 (2009).
12. T. J. Davidson, F. Kloosterman, M. A. Wilson, *Neuron* **63**, 497 (2009).
13. A. S. Gupta, M. A. van der Meer, D. S. Touretzky, A. D. Redish, *Neuron* **65**, 695 (2010).
14. M. A. Wilson, B. L. McNaughton, *Science* **265**, 676 (1994).
15. G. Buzsáki, *Cereb. Cortex* **6**, 81 (1996).
16. H. S. Kudrimoti, C. A. Barnes, B. L. McNaughton, *J. Neurosci.* **19**, 4090 (1999).
17. G. Girardeau, K. Benchenane, S. I. Wiener, G. Buzsáki, M. B. Zugaro, *Nat. Neurosci.* **12**, 1222 (2009).
18. V. Ego-Stengel, M. A. Wilson, *Hippocampus* **20**, 1 (2010).
19. D. Dupret, J. O'Neill, B. Pleydell-Bouverie, J. Csicsvari, *Nat. Neurosci.* **13**, 995 (2010).
20. J. O'Neill, B. Pleydell-Bouverie, D. Dupret, J. Csicsvari, *Trends Neurosci.* **33**, 220 (2010).
21. M. F. Carr, S. P. Jadhav, L. M. Frank, *Nat. Neurosci.* **14**, 147 (2011).
22. A. C. Singer, L. M. Frank, *Neuron* **64**, 910 (2009).
23. S. Cheng, L. M. Frank, *Neuron* **57**, 303 (2008).
24. S. M. Kim, L. M. Frank, *PLoS ONE* **4**, e5494 (2009).

25. See supplementary materials on *Science* Online.
26. A. C. Smith *et al.*, *J. Neurosci.* **24**, 447 (2004).
27. G. Dragoi, K. D. Harris, G. Buzsáki, *Neuron* **39**, 843 (2003).
28. J. O'Neill, T. J. Senior, K. Allen, J. R. Huxter, J. Csicsvari, *Nat. Neurosci.* **11**, 209 (2008).
29. D. Reisel *et al.*, *Nat. Neurosci.* **5**, 868 (2002).
30. A. J. Murray *et al.*, *Nat. Neurosci.* **14**, 297 (2011).

Acknowledgments: Supported by a Wheeler Center Fellowship (S.P.J.), a Helen Hay Whitney Foundation grant (C.K.), and NIH grant RO1 MH080283. The authors declare no competing financial interests.

Supplementary Materials
www.sciencemag.org/cgi/content/full/science.1217230/DC1
Materials and Methods
Supplementary Text
Figs. S1 to S20
References (*31*–*35*)

29 November 2011; accepted 16 April 2012
Published online 3 May 2012;
10.1126/science.1217230

Segregation of Axonal and Somatic Activity During Fast Network Oscillations

Tamar Dugladze,[1] Dietmar Schmitz,[2,3,4] Miles A. Whittington,[5] Imre Vida,[4] Tengis Gloveli[1,3]*

In central neurons, information flows from the dendritic surface toward the axon terminals. We found that during in vitro gamma oscillations, ectopic action potentials are generated at high frequency in the distal axon of pyramidal cells (PCs) but do not invade the soma. At the same time, axo-axonic cells (AACs) discharged at a high rate and tonically inhibited the axon initial segment, which can be instrumental in preventing ectopic action potential back-propagation. We found that activation of a single AAC substantially lowered soma invasion by antidromic action potential in postsynaptic PCs. In contrast, activation of soma-inhibiting basket cells had no significant impact. These results demonstrate that AACs can separate axonal from somatic activity and maintain the functional polarization of cortical PCs during network oscillations.

In response to synaptic inputs, action potentials (APs) are generated at the axon initial segment (AIS) and propagate along the axon to provide an output signal (*1*, *2*). However, APs can also be initiated in the distal axon under certain conditions (*3*–*7*), but it is unknown how back-propagation of such ectopic APs (EAPs) to the somatodendritic compartment is controlled.

We performed patch-clamp recordings from the soma or axon of hippocampal CA3 pyramidal cells (PCs) during fast network oscillations. In parallel, we monitored the local field potential in the stratum pyramidale (Fig. 1 and fig. S1). During gamma-frequency activity, CA3 PCs discharged phase-locked with the oscillations, but only at a low frequency (*8*–*10*) of 3.5 ± 0.5 Hz (Fig. 1A). Unexpectedly, the frequency of action currents (ACs) in axons recorded >600 μm from the soma was higher by a factor of 4 to 5, with a mean frequency of 16.1 ± 1.4 Hz (Fig. 1, B and C). These results indicate that in the distal axon of PCs, EAPs are generated at high frequencies during gamma oscillations; however, most of these APs do not reach the somatodendritic compartment. To directly demonstrate that axonal spikes are ectopically generated and fail to invade the soma, we performed dual somatic and axonal cell-attached recordings from individual cells (Fig. 1, D to F). We again found a low discharge frequency in the soma (2.7 ± 0.5 Hz) but a considerably higher frequency in the axon (15.8 ± 0.7 Hz; n = 9 cells) (Fig. 1, E and F).

The absence of EAP invasion of the soma may reflect strong γ-aminobutyric acid type A ($GABA_A$) receptor ($GABA_AR$)–mediated inhibition in the soma or at the AIS of PCs. We therefore applied $GABA_AR$ antagonist during dual axonal and somatic recordings from PCs. Bath application of $GABA_AR$ antagonist gabazine considerably increased the probability of the back-propagation of antidromic APs (from 19.3 ± 2.9% to 91.2 ± 1.2%, before and after gabazine application, respectively; n = 3) (fig. S2, A to C). Somatic invasion of APs in the presence of gabazine was maintained during hyperpolarization to –90 mV (92.7 ± 1.8%; n = 3), further indicating that APs are initiated antidromically in the distal axon. These results provide evidence that $GABA_AR$-mediated inhibition effectively controls axosomatic coupling and prevents the back-propagation of EAPs to the soma.

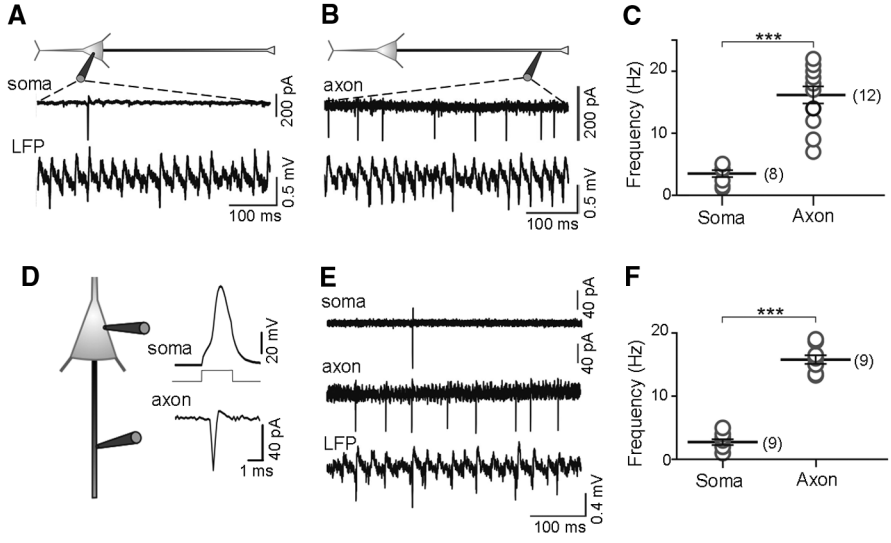

Fig. 1. High-frequency discharge of the axon, but not the soma, of hippocampal CA3 pyramidal cells during gamma-frequency oscillations in vitro. (**A** and **B**) Schematic representation of the recording configuration (top). Somatic (A) and axonal (B) cell-attached patch-clamp recordings were obtained from PCs during kainic acid (KA)–induced gamma oscillations in the local field potential (LFP). (**C**) Summary plot of AC frequency in the soma (8 cells) and axon (12 cells) reveals a significant difference between the two compartments (***P < 0.0001). (**D**) Scheme of dual somatic and axonal recording configuration. APs evoked in whole-cell configuration by brief depolarizing current injection into the soma (800 pA) (inset) reliably induced ACs in the axon, confirming that recordings are made from two compartments of the same cell. (**E**) Dual somatic and axonal cell-attached recordings directly demonstrate that high-frequency axonal spikes fail to invade the soma during gamma-frequency oscillations (LFP). (**F**) Summary plot shows the highly significant difference in the discharge frequency observed at the soma and proximal axon in dual recordings (n = 9 cells) during network oscillations.

[1]Institute of Neurophysiology, Charité-Universitätsmedizin Berlin, Charitéplatz 1, 10117 Berlin, Germany. [2]Neuroscience Research Center, Charité-Universitätsmedizin Berlin, Charitéplatz 1, 10117 Berlin, Germany. [3]Bernstein Center for Computational Neuroscience Berlin, Unter den Linden 6, 10099 Berlin, Germany. [4]Cluster of Excellence, NeuroCure, Charitéplatz 1, 10117 Berlin, Germany. [5]Institute of Neuroscience, Medical School, University of Newcastle, Framlington Place, Newcastle upon Tyne NE2 4HH, UK.

*To whom correspondence should be addressed. E-mail: tengis.gloveli@charite.de

www.sciencemag.org/cgi/content/full/science.1217230/DC1

Supporting Online Material for

Awake Hippocampal Sharp-Wave Ripples Support Spatial Memory

Shantanu P. Jadhav, Caleb Kemere, P. Walter German, Loren M. Frank*

*To whom correspondence should be addressed. E-mail: loren@phy.ucsf.edu

Published 3 May 2012 on *Science* Express
DOI: 10.1126/science.1217230

This PDF file includes:

Materials and Methods

Experimental overview and pre-training

A total of 14 male Long Evans rats weighing 450-600 grams were used in this study. 10 animals were used for combined recording (local field potentials and spiking activity) and stimulation experiments (n = 6, 4 respectively for SWR disruption and control stimulation). 4 additional animals were used to collect only behavior data (un-implanted group). All procedures were approved by the Institutional Animal Care and Use Committee at the University of California, San Francisco and conformed to National Institutes of Health guidelines (*11*, *24*). Animals were first habituated to daily handling over several weeks. After habituation, animals were food deprived to 85-90% of their baseline weight and pre-trained to run back and forth on a raised linear track for liquid food rewards (evaporated milk) which were automatically dispensed in food wells (triggered by breaking an IR beam) at each end of the track. Animals were trained on the linear track for two 15-minute sessions per day with intervening 15-minute rest periods to habituate them to the eventual experimental design (Fig. 1F) and were trained to a criterion level of at least 50 food-well visits per 15-minute session on the linear track prior to surgical implantation and recording-stimulation on the W-track (see below). Following recovery from surgery and electrode placements, animals were food-deprived and retrained on the linear track with the recording cables attached for at least two days before the W-track sessions started. Following the conclusion of the experiments, we made micro-lesions through each electrode tip to mark recording locations (30 μA for 3 sec). After receiving an overdose of Euthanasol, animals were perfused intracardially with isotonic sucrose and 4% PFA. The brains were stored in PFA, frozen, and cut coronally at 50 μm sections, and stained with cresyl violet.

Surgical implantation and electrode placements

Surgical implantation procedures were as previously described (*11*). Animals were implanted with a microdrive array with 12 independently moveable tetrodes (groups of four twisted 12.5 μm nichrome wires) assembled in a bundle targeting right dorsal hippocampal region CA1 (-3.6 mm AP and 2.2 mm ML) and one or two moveable bipolar stimulation electrodes targeting vHC (-1.3 mm AP and ±1 mm ML). The bipolar electrodes (10 kΩ tungsten stimulating electrodes,) consisted of two electrodes in either a stereotrode configuration inserted on the ipsilateral side (relative to the CA1 tetrodes) or inserted bilaterally. We used a bipolar stimulating electrode configuration as this limits current spread compared with stimulating through a unipolar electrode relative to a distant ground. We used 0.2 ms biphasic stimulation pulses applied across the two electrodes. Stimulation electrodes were adjusted to a depth of 3.8 mm relative to bregma and micro-adjusted as needed for optimal disruption of hippocampal activity for ~100 ms with minimal stimulation amplitude during a calibration procedure prior to experimentation. Biphasic stimulation waveforms minimize damage at the site of stimulation and we found that the same stimulation amplitude was usually effective throughout the course of the 8 days. We measured evoked field responses in CA1 with 0.1 Hz probe stimulation in the rest periods before and after behavior (Fig. 1F) using the same stimulation amplitudes as those used for disruption in the intervening behavior run sessions for each day. On the days following surgery, hippocampal tetrodes were advanced to the cell layers until characteristic EEG patterns (sharp wave polarity, theta modulation) and neural firing patterns indicated that the target regions

had been reached. All spiking activity was recorded relative to a reference tetrode located in the corpus callosum. Tetrode positions were adjusted after daily recording sessions if necessary, but never within 4 hrs before recording sessions.

Behavior and recording-stimulation

Prior to each experiment, stimulation amplitude was calibrated to detect the minimal stimulation amplitude leading to ~100 ms inhibition of multi-unit spiking activity in CA1. Single-pulse electrical stimulation consisted of 0.2 ms biphasic pulses applied to the bipolar electrodes. The amplitudes used were in the range 40-180 μA. The level of current was always held constant across multiple sessions recorded in a single day, and the same amplitude was effective across all days for most animals.

Animals were tested on the W-track continuous alternation task for 8 days, in two 15-minute sessions per day. The W-track was novel on the first day and had dimensions of 76 x 76 cm with 7 cm wide track sections (Fig. 1). All three arms had reward food wells at their endpoints, and evaporated milk rewards were automatically delivered in the food wells. Rewards were delivered according to the following rules (*24*). (1) A visit to the center food well was rewarded when the rat came from either side food well. (2) A visit to the left or right food well was rewarded when the rat came from the center food well after having previously visited the opposite side food well. (3) Consecutive repeat visits to the same food well were never rewarded. At the beginning of each session, the experimenter placed the rat on the center arm facing the center food well, which was pre-baited with reward. At the end of each run session, animals were transferred to the familiar rest box (15 minute rest periods, floor 34 x 34 cm; walls, 50 cm).

Data were collected using the NSpike data acquisition system (*11*) (L.M.F. and J. MacArthur, Harvard Instrumentation Design Laboratory). We recorded continuous local field potentials (LFP, filtered 0.5-400 Hz and sampled at 1500 Hz) from all tetrodes (one channel was chosen from each tetrode for LFP recording). Spike data were sampled at 30 kHz, digitally filtered between 600 Hz and 6 kHz (2 pole Bessel for high and low pass) and threshold crossing events were saved to disk (40 samples at 30 kHz). An infrared light emitting diode array with a large and a small cluster of diodes was attached to the preamps during recording. Behavior sessions were recorded with an overhead monochrome CCD camera (30 fps and a resolution of 0.45 cm/ pixel) and the animal's position and speed were detected online using the infrared diodes. A separate camera mounted over the rest box was used for recording rest sessions.

Real-time detection algorithm. Field potential signals from the 5-6 tetrodes chosen for online detection were broadly filtered in the ripple band (20 tap band-pass IIR filter, 100-400 Hz). In order to establish a disruption threshold, we calculated smoothed values of the mean and s.d. of the absolute value of the filtered LFP signal on each tetrode being used for detection using an iterative procedure:

$$\mu_{est}(n) = \mu_{est}(n-1) \cdot (N_{smooth} - 1)/N_{smooth} + |x| / N_{smooth}$$

$$\sigma_{est}(n) = (|\, |x| - \mu_{est}(n-1)\,| - \sigma_{est}(n-1))/N_{smooth} + \sigma_{est}(n-1)$$

Here μ_{est} and σ_{est} are the estimated mean and s.d. of the absolute value of the filtered LFP, x, and N_{smooth} is the number of samples for smoothing (typically 10000). We allowed these estimates to stabilize before each run session. To generate a smoothened estimate of the envelope (v_{est}) of the filtered LFP, we used the following iterative estimator:

$$v_{est}(n) = v_{est}(n\text{-}1) + g_i(n\text{-}1) \cdot (|x| - v_{est}(n\text{-}1))$$

To allow for rapid detection of increases in power, we used a larger gain, g_i, for periods when the envelope was increasing: when the envelope was decreasing ($|x| \leq v_{est}$), $g_i = 0.2$; when the envelope was increasing, we used a moving average of the last 19 values of g_i and 1.2:

$$g_i(n) = 0.2, \qquad \text{for } |x| \leq v_{est}(n\text{-}1)$$

$$= \langle g_i(n\text{-}20), g_i(n\text{-}19), \ldots, g_i(n\text{-}1), 1.2) \rangle, \qquad \text{for } |x| > v_{est}(n\text{-}1)$$

The threshold for disruption was set to 4-6 s.d. above the mean. To prevent false-positives, vHC stimulation was triggered only when the smoothed LFP envelope exceeded threshold on at least 2 tetrodes. Stimulation rate was limited to a maximum of 4 Hz by enforcing a lock-out period of 250 ms after each stimulation event. We also implemented an online speed filter to estimate the speed of the animal in real-time using online tracking of the diodes. The real-time, causal speed filter was implemented as a one-sided Gaussian with a standard deviation of 0.5 sec and a total length of 3 secs. This corresponds to one-half the Gaussian that was used to estimate speed of the animal during post-hoc analysis when we could also smooth over future times. We used the speed filter to prevent false-positive stimulation when animals were moving continuously at high-speed (threshold of 5 cm/sec to 10 cm/sec). This filter is effective only during continuous running at high speeds and not during sudden accelerations due to causality of the filter.

For control stimulation animals, a latency of 150-200 ms was introduced between online detection and onset of stimulation. For 3 of the control animals, we switched to SWR disruption for two further days (days 9 and 10) after the regular 8 day period was over.

Behavior analysis

During post-hoc analysis, the rat's position on the track was reconstructed using a semi-automated analysis of digital video of the experiment for tracking the front and back diodes with custom-written software. The position extracted from the video was first smoothed using a nonlinear method (*24*) and speed was computed by taking the difference in position and then smoothing with a Gaussian kernel with standard deviation 0.5 s and a total length of 6 seconds. The extracted position was used to parse the running behavior into trials (or, trajectories) and the trajectories were classified as inbound or outbound according to their point of origin on the W-track. All trajectories in which the rat departed either from the left food well or from the right food well were classified as inbound trajectories, and all trajectories in which the rat departed from the center food well were classified as outbound trajectories. Proportion of correct trials and ten-trial moving averages of performance were computed using the trajectory assignments. While this sort of moving average is frequently used to evaluate behavioral performance, it is difficult to compute meaningful confidence bounds for individual animals using this analysis. We therefore used a state-space model of learning (*24, 26*) to estimate individual learning curves for each subject on both the inbound and outbound trials and estimate the learning day and learning trial for each animal. This model uses the observed data to estimate the subject's probability of making a correct choice from trial to trial, along with confidence bounds on that estimated probability. The state-space model-based analysis has a number of advantages over moving average or change-point analyses, including the ability to estimate confidence bounds for individual subjects and greater sensitivity to changes associated with learning. Briefly, this

model describes an animal's choice behavior as an evolving process. At each trial, the model estimates the value of a hidden (e.g. not directly observable) ''state'' variable that represents the probability of making a correct choice. The model simultaneously estimates confidence bounds for the state variable, representing the level of uncertainty about the probability of a correct choice. We used the expectation maximization algorithm to find the set of values that best describe the animal's choice behavior across time. We set the initial baseline probability used by the algorithm to 0.5. The algorithm can also estimate the initial probability and results were similar using this option. Learning trial and learning day for each animal were assigned as the first trial and test day at which the 90% confidence interval of the estimated probability of correct performance exceeded and remained above chance (we used a conservative estimate of 0.5 as chance-level performance) through the remainder of the testing period. One SWR disruption animal failed to reach criterion performance and was assigned the last trial and day number as learning trial and day respectively (fig. S3).

There was no statistical difference between the control stimulation and un-stimulated groups for any measure. All statistical results were similar and stronger when control animals were pooled and compared to the SWR disruption group (n = 8 control animals vs. n = 6 SWR disruption animals), including a *p* value of 0.0007 corresponding to the likelihood that all animals in the SWR interruption group would perform worse than all other animals. Further, in addition to parametric and non-parametric statistical methods, we also used permutation (randomization) tests for statistical comparisons (*31, 32*) and obtained similar significant results (not shown).

Neural analyses

SWRs were detected during post-hoc analysis as described previously (*11, 23*). Raw LFPs recorded from the tetrodes used for online SWR detection were filtered between 150 – 250 Hz and the SWR envelope was determined using a Hilbert transform. The envelope was smoothed with a Gaussian with a s.d. of 4 ms and a width of 32 ms. SWRs were defined as contiguous periods when the smoothed SWR envelope stayed above 3 s.d. of the mean for at least 15 ms on at least one tetrode. Single-unit data was analyzed for 4 animals each in the disruption and control stimulation group. Individual units were identified by clustering spikes in multiple dimensions using custom software (MatClust, M. Karlsson) as previously described (*11*). Putative inter-neurons were identified using standard waveform and mean rate criteria and were excluded from the analysis (*11, 23*). Putative excitatory pyramidal cells were considered as place cells and included in the place-field and reactivation analysis only if they had a linearized peak-rate > 3 Hz (see below) on the maze. Cells that fired only during rest periods were not analyzed. Cluster quality was similar for the place cells in the SWR disruption and control stimulation groups (n = 108 and n = 96 cells, isolation distance (*11*) of 28.2 ± 2.2 and 32.0 ± 3.4 respectively, t-test, $t = 1.47$, $p > 0.14$).

Place-field activity was calculated only when the speed of the animal was > 3 cm/sec and all SWRs and stimulation times were excluded. Two-dimensional occupancy-normalized spatial rate maps (Figs. 3, 4 and figs. S10, S11) were constructed with 2-cm square bins of spike count and occupancy, both smoothed with a two-dimensional Gaussian (8-cm s.d.). To measure place field locations and overlap, we calculated the linearized activity of each cell. The rat's linear position was measured as the distance in centimeters along the track from the reward site on the center arm. We then produced an occupancy-normalized firing-rate map for each of the 4 linear trajectories (2 outbound and 2 inbound, fig. S11) using spike counts and occupancies calculated

in 2-cm bins and smoothed with a 4-cm s.d. Gaussian curve. The place field peak rate (Fig. 3C) was defined as the maximum rate across all spatial bins. A peak rate of 3 Hz or greater was required for a cell to be considered a place cell and included in subsequent analysis. Place field stability was defined as the correlation between the linearized place fields (for all 4 trajectories) of a cell for the two run sessions within a day (Fig. 3B, fig. S11). The proportion of the environment over which each neuron was active (place-field size) was defined as the length of the spatial bins in which the cell fired at > 1 Hz linearized firing rate divided by the total length of the trajectories (averaged across the two run sessions, Fig. 3D). Place field overlap for pairs of cells was defined as twice the sum of the overlapping areas of the linear rate curves divided by the sum of the areas of each curve (averaged across the two run sessions). This measure is bounded between 0 and 1, where 0 signifies no overlap and 1 signifies perfect overlap (*11*) (Fig. 4A, B). For the reactivation analysis (Fig. 4A, B, and fig. S18), cross-correlations during rest periods were calculated using only spikes that occurred during SWRs when the animal was still (speed < 2 cm/sec in the rest box, length of time periods when animals were still in the rest box were equivalent between the two groups of animals, t-test, $p > 0.05$ criterion). Only spike pairs for which at least ten spikes occurred during SWRs were included. Reactivation probability during each rest period was defined as the mean normalized cross-correlation in a 100 ms window (*14*, *16*) (±50 ms around zero time-lag), and the reactivation strength was defined as the difference in reactivation probabilities during the *Post* rest session after the W-track run sessions (averaged across the two rest sessions, post1 and post 2) and the *Pre* rest session before the run sessions. Correlations during run periods were calculated using place-field spikes as described above. Run correlations were quantified using a 200 ms window (±100 ms around zero time-lag, fig. S18).

SOM Text

Real-time SWR disruption during behavior using vHC stimulation

Commissural stimulation is a well-characterized method (*17, 18, 33*) that has been used previously to reset the phase of theta oscillations (*33*) and to specifically disrupt SWRs during post-behavior sleep (*17, 18*). The vHC contains commissural fibers which connect intra-hippocampal networks (CA3-CA3, CA3-DG, DG-DG, and Schaffer collaterals connecting CA3-CA1) across the hemispheres (*17, 33-35*). Single-pulse vHC stimulation leads to a brief, synchronous discharge of large ensembles of principal cells and interneurons throughout both hippocampi and dentate gyri, followed by transient silencing of the hippocampal network (pyramidal cells, granule cells and interneurons) due to a combination of GABA-receptor mediated inhibition, Ca^{2+}-dependent K^{+} conductance increase and dis-facilitation (*17, 33-35*) (also see Fig. 1B-E, fig. S2). The evoked field response in CA1 and length of transient inhibition increases with the stimulation amplitude. Previous studies have reported transient inhibition of intra-hippocampal activity for 50-250 ms using single-pulse vHC stimulation with no effect on activity in output entorhinal cortical and pre-frontal cortical areas. Hippocampal activity returns to normal after recovery from inhibition (*17, 33*). Thus, as a method for transiently inhibiting intra-hippocampal activity, vHC stimulation offers the advantage of targeting a large part of the hippocampal circuit by acting locally on the commissural axonal bundle while maintaining temporal specificity. Further, since SWRs are of the order of ~100 ms, single-pulse vHC stimulation is ideally suited for disrupting SWRs (*17*). We calibrated the stimulation amplitude for each animal to find the minimum amplitude leading to inhibition of multi-unit spiking activity in CA1 for ~100 ms using a biphasic pulse length of 0.2 ms (Methods, Fig. 1C-E, fig.S2).

SWRs are seen primarily during consummatory behaviors, immobility and low speed movement (*15, 21*), although they also occur during exploratory periods (*8, 21*). We detected SWRs in real-time simultaneously on 5-6 tetrodes in CA1 with a criterion of threshold crossings of SWR power on at-least two tetrodes to avoid false positives. An online speed filter was also used to prevent false-positive stimulation when animals were running continuously at high speed (*25*). Real-time detection triggered vHC stimulation and SWR oscillations were terminated within 25 ms of onset as determined by post-hoc analysis (Fig. 1B-D, fig. S2). In the control stimulation group, vHC stimulation was delayed by 150-200 ms after real-time detection of SWRs. This ensured that the control group animals received the same number of stimulations and that these stimulation events occurred when animals were in a similar behavior state as animals in the disruption group (figs. S14-17). In both groups, we limited our instantaneous stimulation rate to 4 Hz by enforcing a lockout period of 250 ms after each stimulation event (*25*), and the mean stimulation rate was even lower (fig. S14). It is unlikely that this low stimulation rate and non-periodic triggering of the stimulation could cause plasticity of synaptic connections in hippocampal circuits. However, there is still a possibility that if SWRs are a privileged period for inducing plasticity in the circuit, then vHC stimulation during SWRs could lead to plasticity that differs from that induced by stimulation in non-SWR periods, which could contribute to observed learning deficits. Previous studies that disrupted sleep SWRs did not control for this possibility (*17, 18*). Thus, we monitored evoked field responses to 0.1 Hz probe stimulations in intervening rest periods. We found no evidence of plasticity in the evoked field

responses (Fig. 3E). Further, place-fields were stable when compared across run sessions within a day (Fig. 3A, B, fig. S10), which also suggests that plasticity was not induced (*27*). We can also rule out any long-term deleterious effect of SWR disruption during behavior for several reasons: the specificity of the observed deficit (Fig. 2), the absence of changes in other behavioral variables (figs. S12-13), the intact place-field activity during behavior (Fig.3, fig. S10), and the absence of any discernible difference in SWR rate and SWR-related reactivation after behavior (Fig.4, fig. S18) between control and disrupted animals. These results indicate that the observed effects can be attributed specifically to a loss of awake hippocampal SWRs.

Acknowledgements

We thank C. Lykken and S. Harris for assistance with histology, A. Nathe for pilot experiments targeting vHC, and all members of the Frank laboratory for comments on the manuscript.

Author Contributions

S.P.J, C.K and L.M.F designed the study. C.K and L.M.F implemented the real-time detection algorithm. S.P.J performed the majority of the experiments with assistance from C.K and P.W.G, and analyzed the data. L.M.F supervised the data collection and analysis. S.P.J and L.M.F wrote the paper with feedback from all the authors.

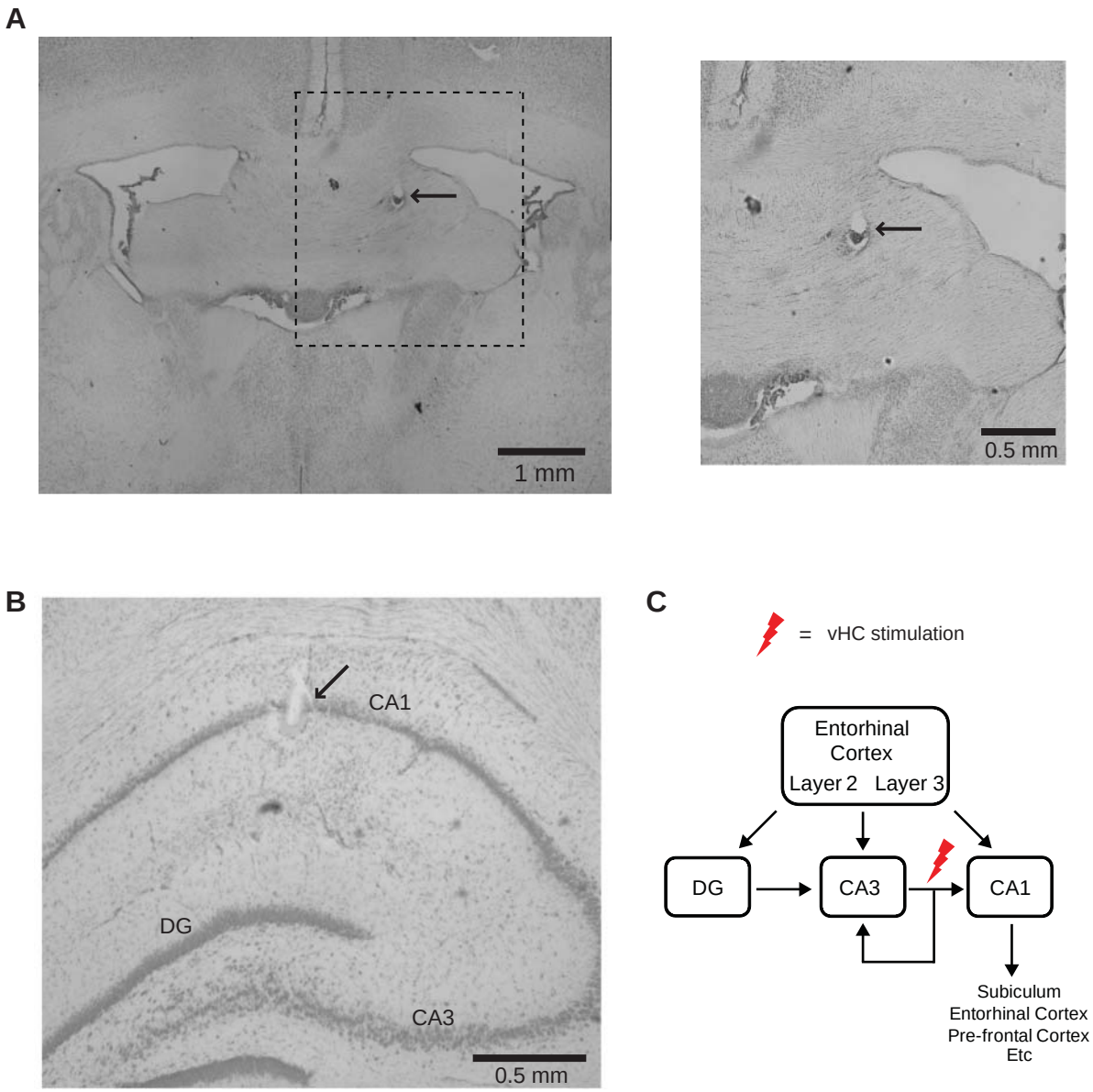

Fig. S1: Stimulation and recording locations. (A, B) Histological sections illustrating stimulation and recording locations. (**A)** Coronal Nissl-stained section illustrating lesion location (marked by arrow) at the end of a stimulation electrode track in the ventral hippocampal commissure (vHC). Area marked by rectangle is expanded on the right. (**B)** Coronal Nissl-stained section illustrating lesion location (marked by arrow) at the end of a tetrode track in CA1 in dorsal hippocampus. CA3 and dentate gyrus (DG) areas are also indicated. (**C)** Schematic illustrating vHC stimulation location in a simplified hippocampal circuit. In addition to CA3-CA1 fibers illustrated in the schematic, the vHC contains commissural fibers connecting CA3-CA3, CA3-DG and DG-DG.

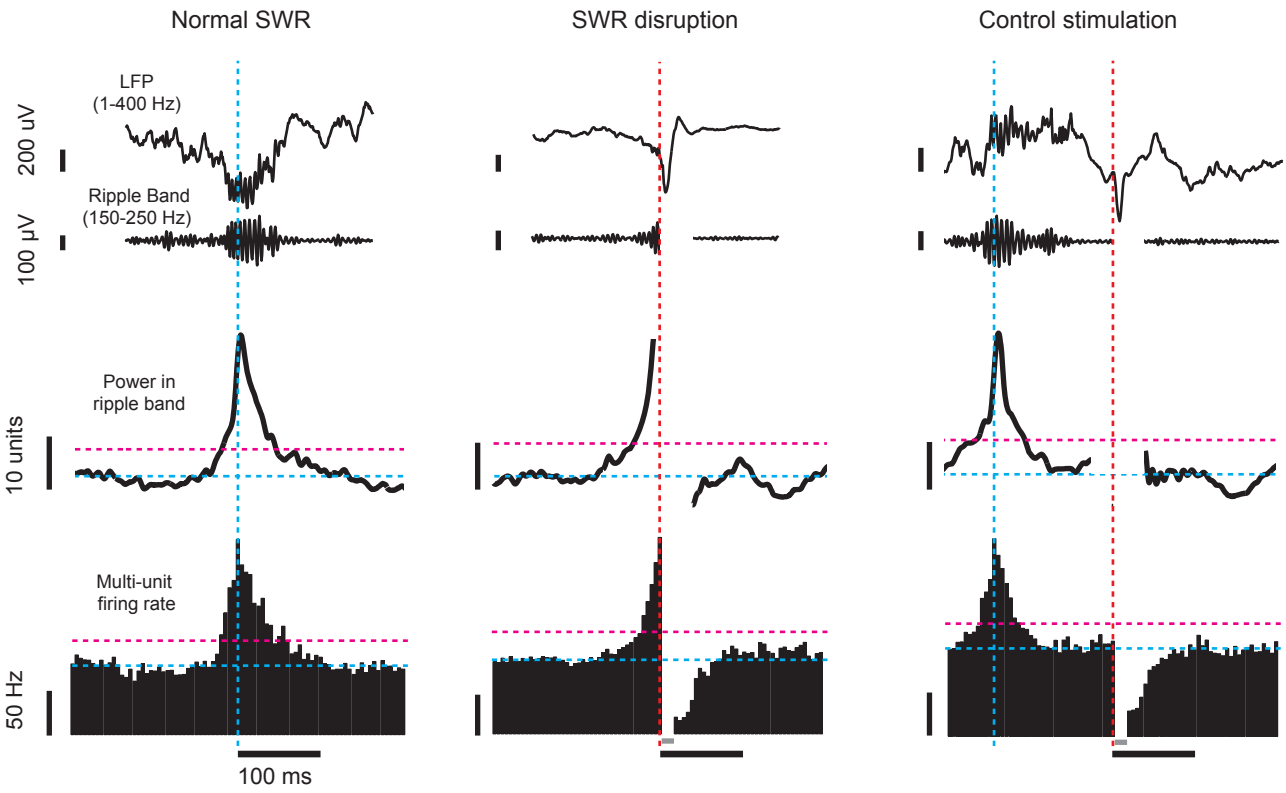

Fig. S2: SWR disruption and control stimulation. Examples for a normal SWR *(Left*), disrupted SWR *(Middle*) and control stimulation after SWR *(Right*). The top row in each panel shows an example of a detected SWR in the broadband LFP (1-400 Hz) and ripple band (150-250 Hz). Vertical cyan lines show the time at which the SWR was detected online by the real-time algorithm and vertical red lines show the time of stimulation. SWR detection and stimulation occurred simultaneously for SWR disruption, and with a delay of 150-200 ms for control stimulation. The middle row shows mean power in the ripple band aligned to all detected SWRs in the run session (n = 576, n = 668, n = 651 SWRs for *Left*, *Middle* and *Right* panels respectively). The bottom row shows mean multi-unit firing rate on the 6 tetrodes used for SWR detection aligned to time of detection for all SWRs in the run session. Horizontal cyan lines in the middle and bottom rows denote baseline ripple power and baseline multi-unit firing rate repectively, and horizontal magenta lines denote 5 standard deviations above mean. Electrical artifacts precluded measurement of ripple band signal (gaps in plot) and multi-unit firing rate (gray bars below x-axis) for a brief period (40 ms for ripple power and 15 ms for multi-unit activity respectively) after stimulation.

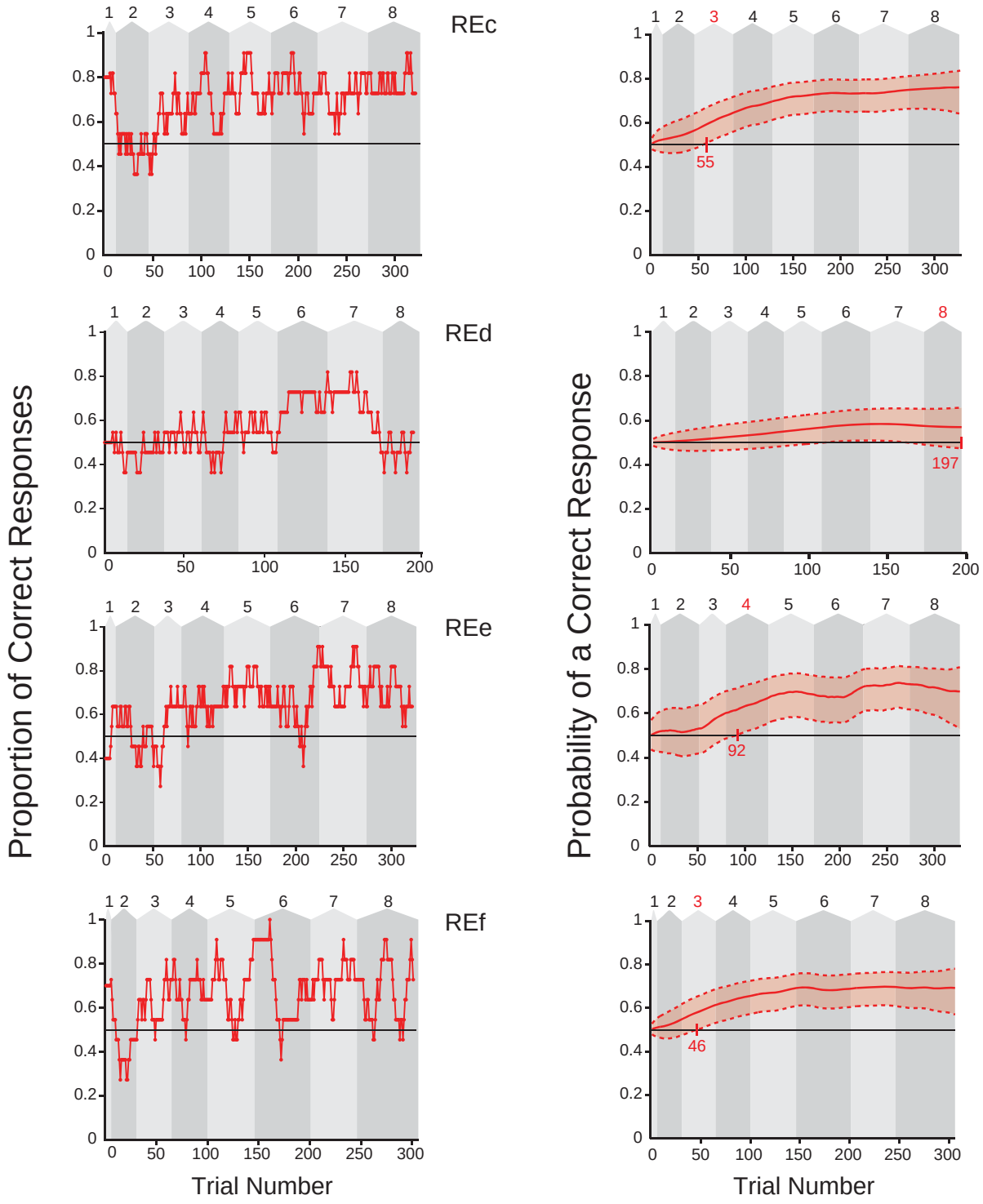
REc
REd
REe
REf
Proportion of Correct Responses
Probability of a Correct Response
Trial Number
Trial Number
55
197
92
46

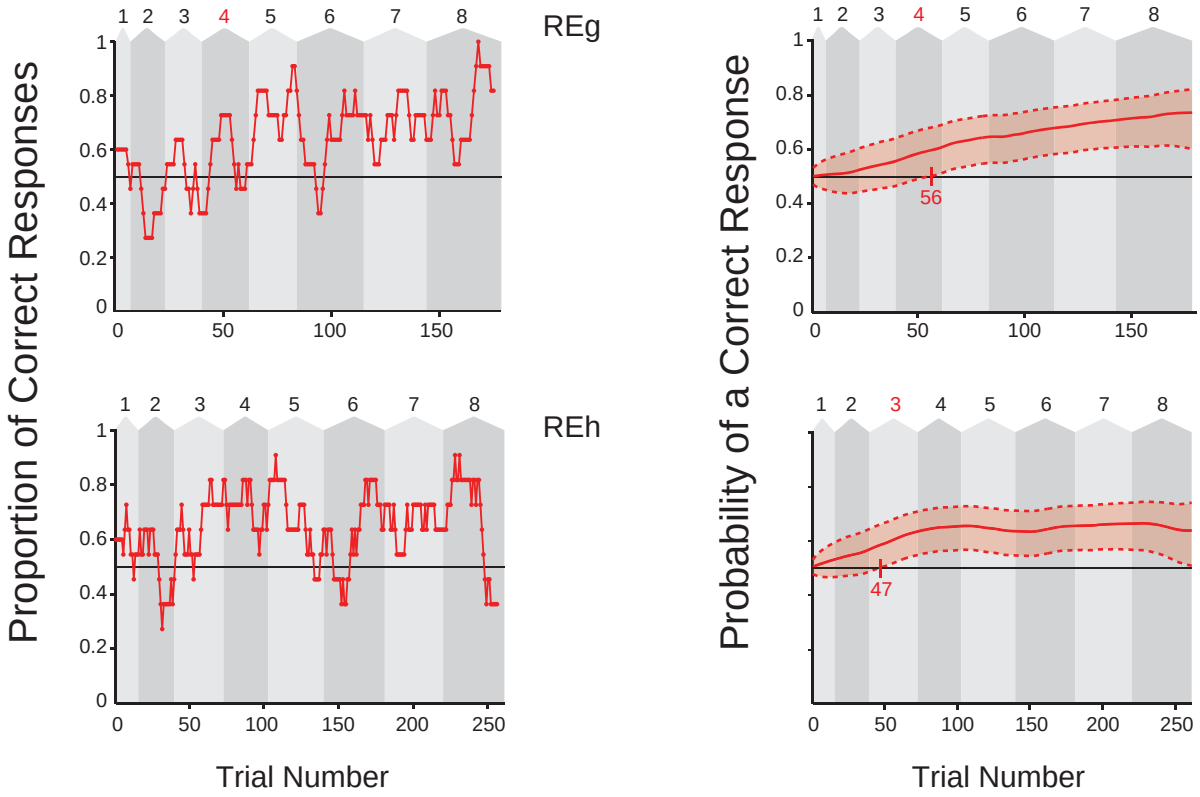

Fig. S3: Outbound behavior in the SWR disruption group. 10-trial moving averages of outbound task performance (*Left*) and corresponding estimated learning curves with confidence intervals (*Right*) for all four animals in the SWR disruption group. For each panel, alternating light and dark gray shaded areas in the background denote days (day numbers on top) across which behavior was measured. Learning trial and learning day are highlighted in red in the panels on right. Names in center identify each individual animal.

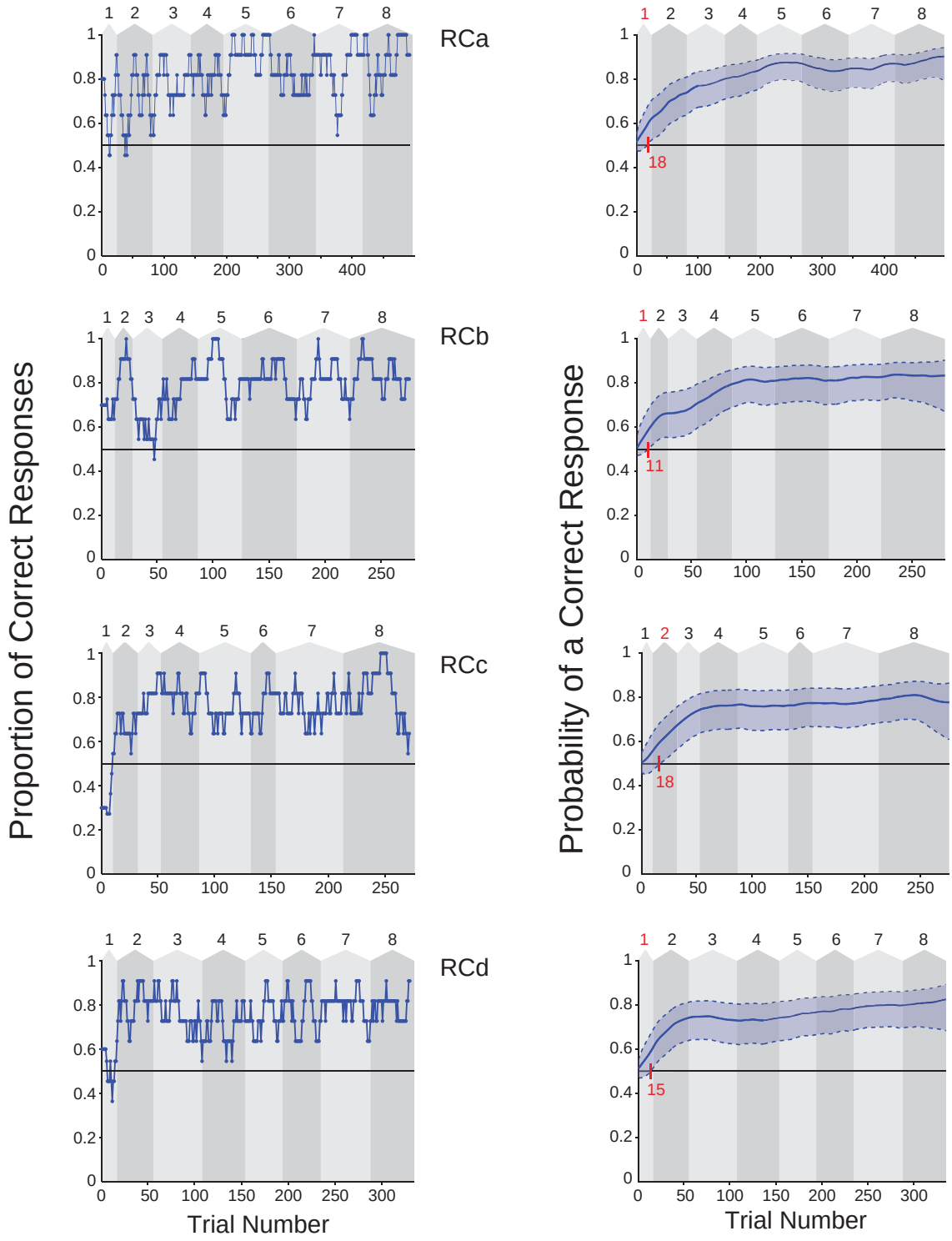

Fig. S4: Outbound behavior in the control stimulation group. 10-trial moving averages of outbound task performance (*Left*) and corresponding estimated learning curves with confidence intervals (*Right*) for all four animals in the control stimulation group. For each panel, alternating light and dark gray shaded areas in the background denote days (day numbers on top) across which behavior was measured. Learning trial and learning day are highlighted in red in the panels on right. Names in center identify each individual animal.

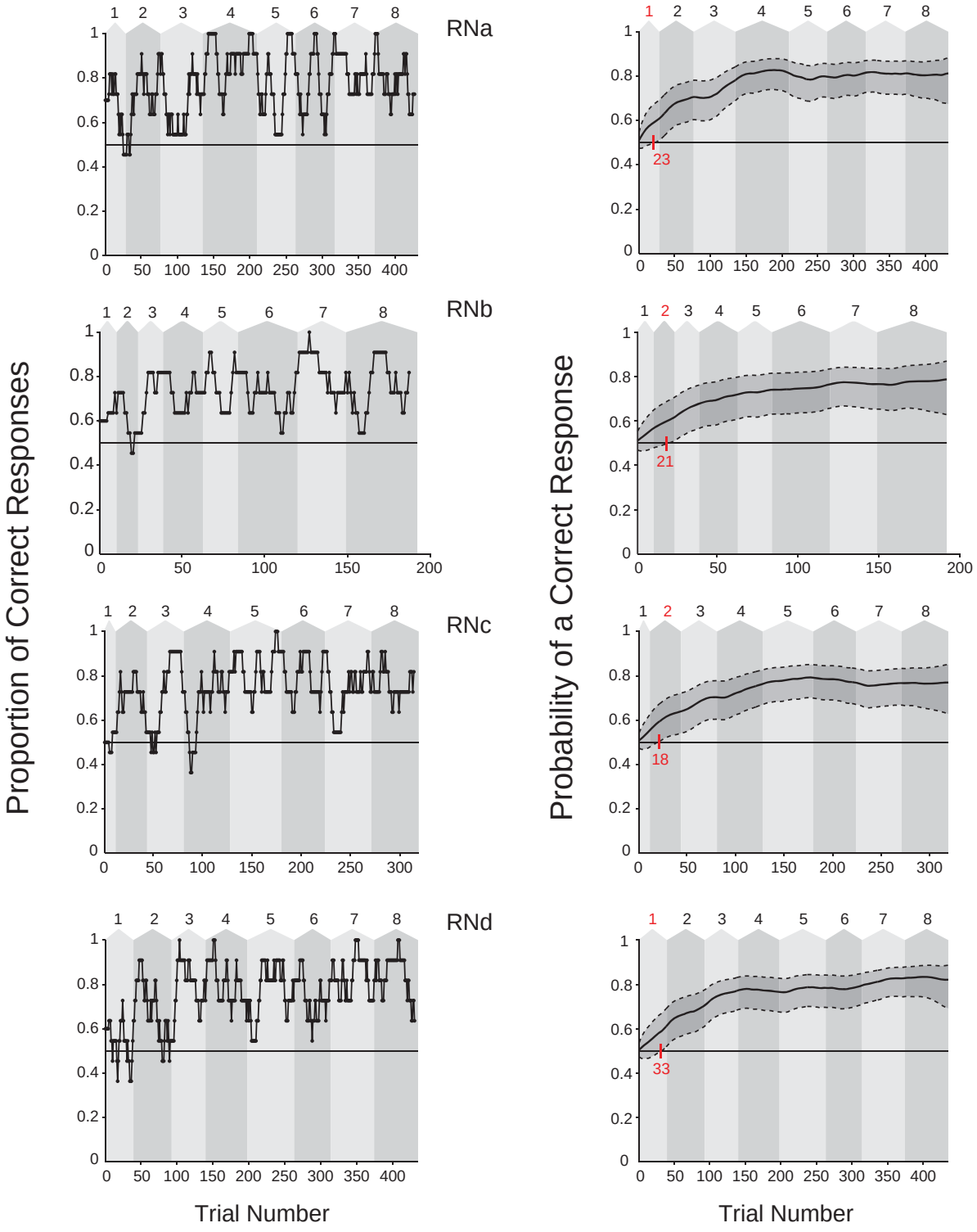

Fig. S5: Outbound behavior in the un-stimulated group. 10-trial moving averages of outbound task performance (*Left*) and corresponding estimated learning curves with confidence intervals (*Right*) for all four animals in the un-implanted, un-stimulated group. For each panel, alternating light and dark gray shaded areas in the background denote days (day numbers on top) across which behavior was measured. Learning trial and learning day are highlighted in red in the panels on right. Names in center identify each individual animal.

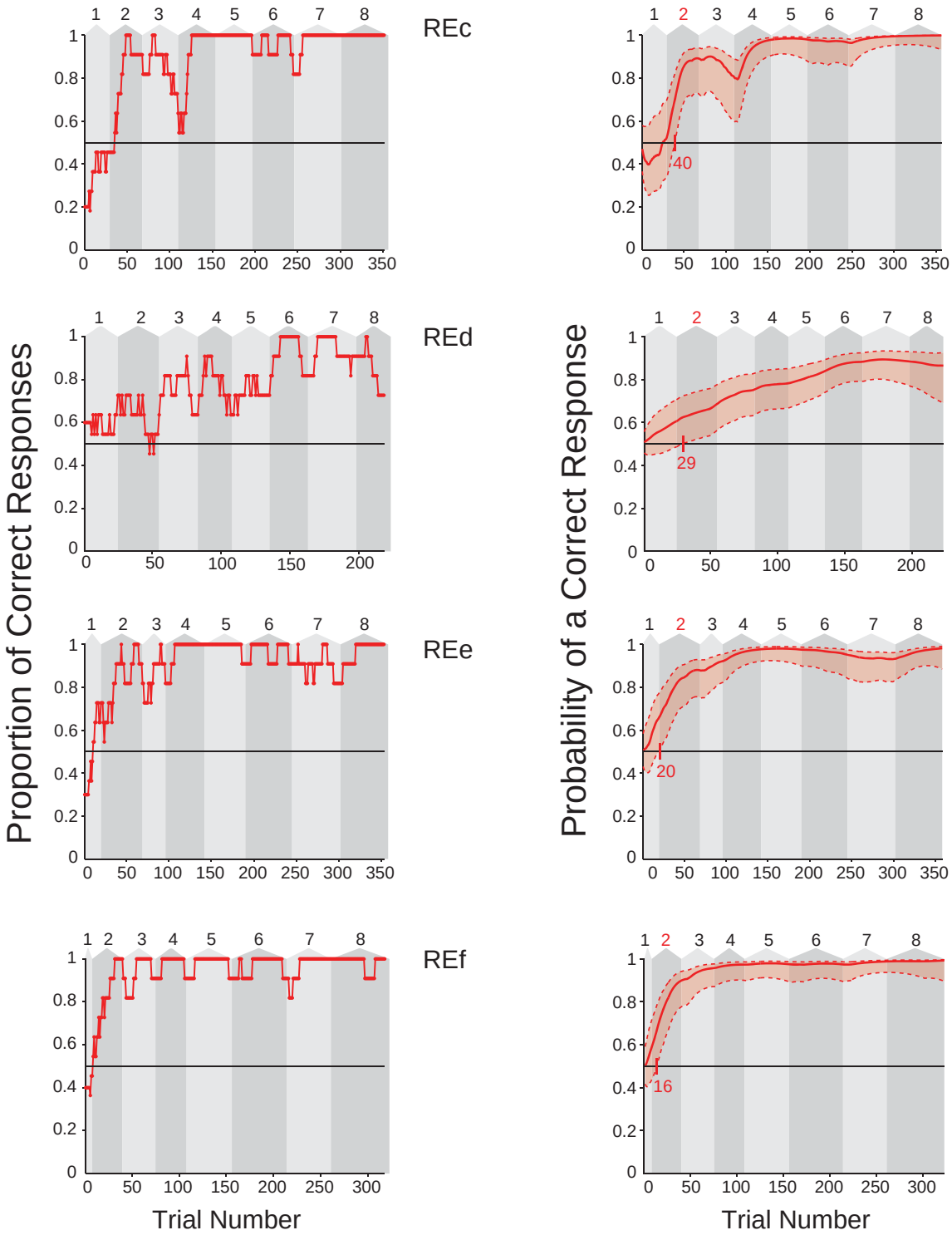
REc
REd
REe
REf
Proportion of Correct Responses
Probability of a Correct Response
Trial Number
Trial Number
40
29
20
16

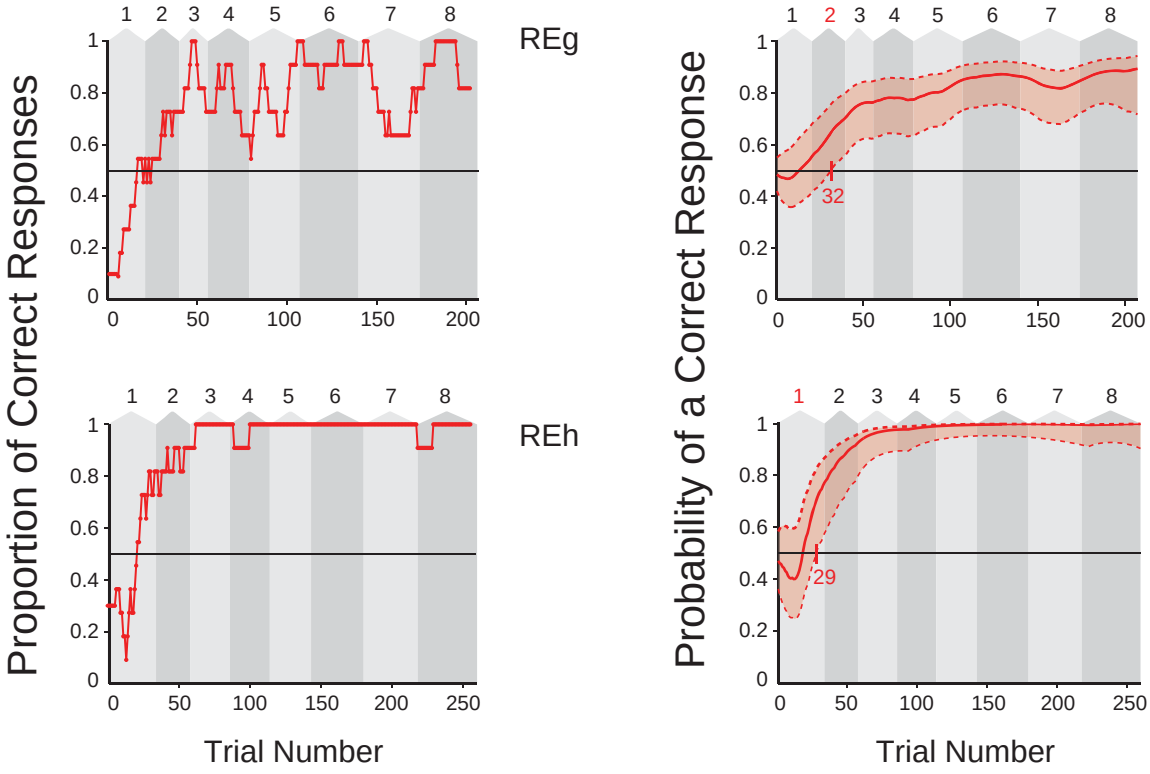

Fig. S6: Inbound behavior in the SWR disruption group. 10-trial moving averages of inbound task performance (*Left*) and corresponding estimated learning curves with confidence intervals (*Right*) for all four animals in the SWR disruption group. For each panel, alternating light and dark gray shaded areas in the background denote days (day numbers on top) across which behavior was measured. Learning trial and learning day are highlighted in red in the panels on right. Names in center identify each individual animal.

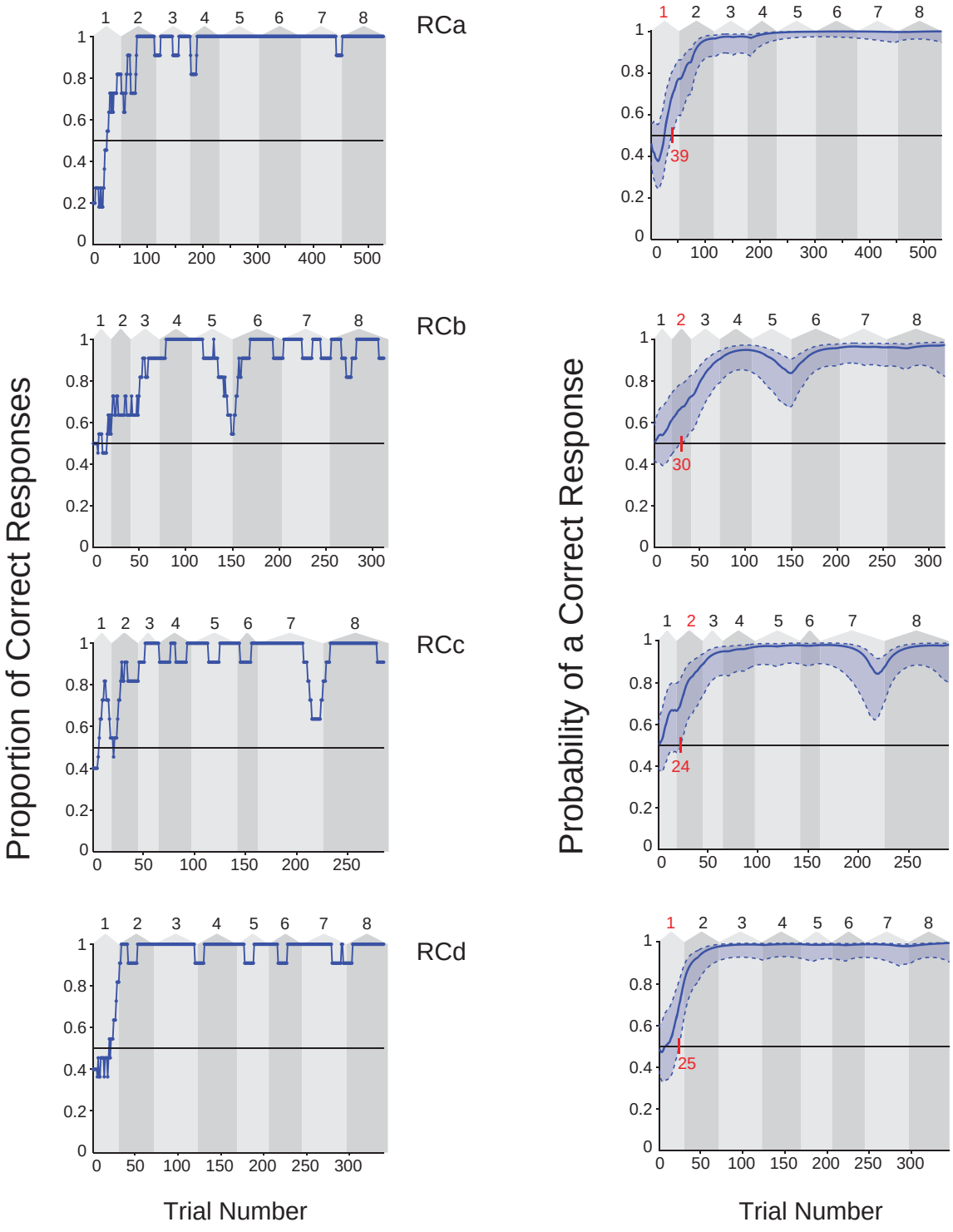

Fig. S7: Inbound behavior in the control stimulation group. 10-trial moving averages of inbound task performance (*Left*) and corresponding estimated learning curves with confidence intervals (*Right*) for all four animals in the control stimulation group. For each panel, alternating light and dark gray shaded areas in the background denote days (day numbers on top) across which behavior was measured. Learning trial and learning day are highlighted in red in the panels on right. Names in center identify each individual animal.

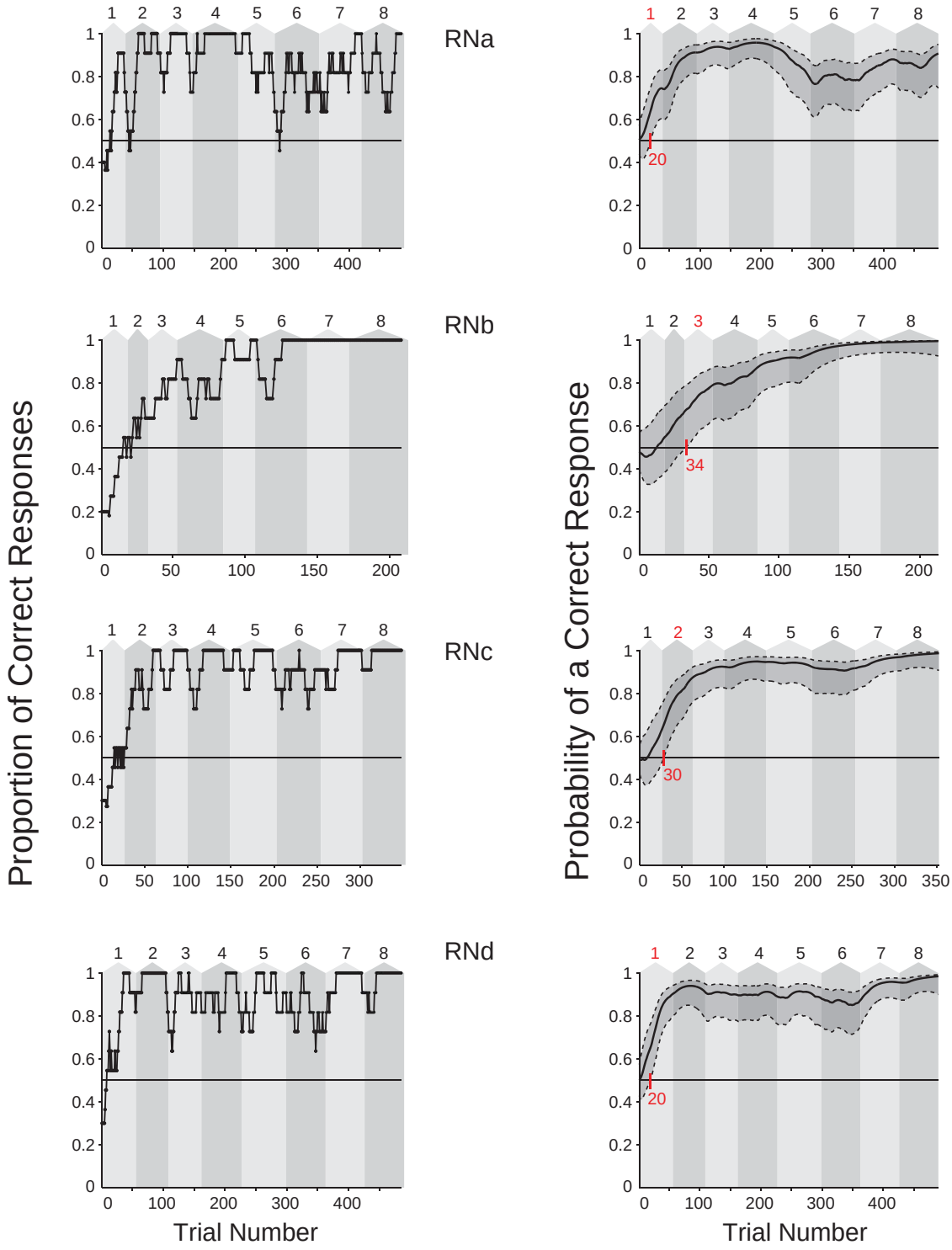

Fig. S8: Inbound behavior in the un-stimulated group. 10-trial moving averages of inbound task performance (*Left*) and corresponding estimated learning curves with confidence intervals (*Right*) for all four animals in the un-implanted, un-stimulated group. For each panel, alternating light and dark gray shaded areas in the background denote days (day numbers on top) across which behavior was measured. Learning trial and learning day are highlighted in red in the panels on right. Names in center identify each individual animal.

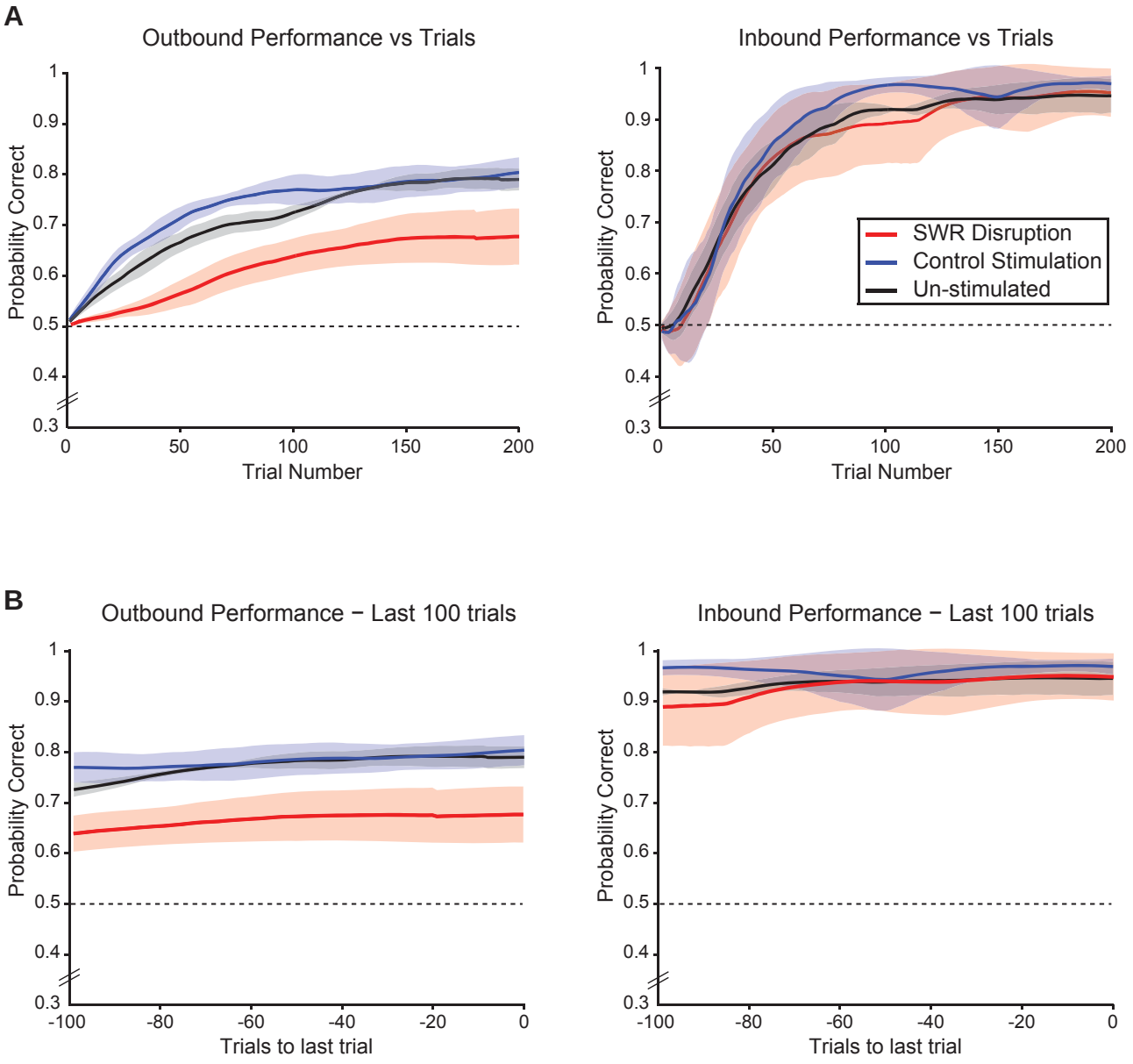

Fig. S9: Learning curves aligned by trial number. (A) Average estimated learning curves for the three groups of animals aligned by trial number (starting with the first trial on day 1 for each animal) for the first 200 outbound (*Left*) and inbound (*Right*) trials. Shaded areas represent standard deviation. (**B)** Average estimated learning curves for the three groups of animals aligned by trial number (ending with the last trial on day 8 for each animal) for the last 100 outbound (*Left*) and inbound (*Right*) trials. Shaded areas represent standard deviation.

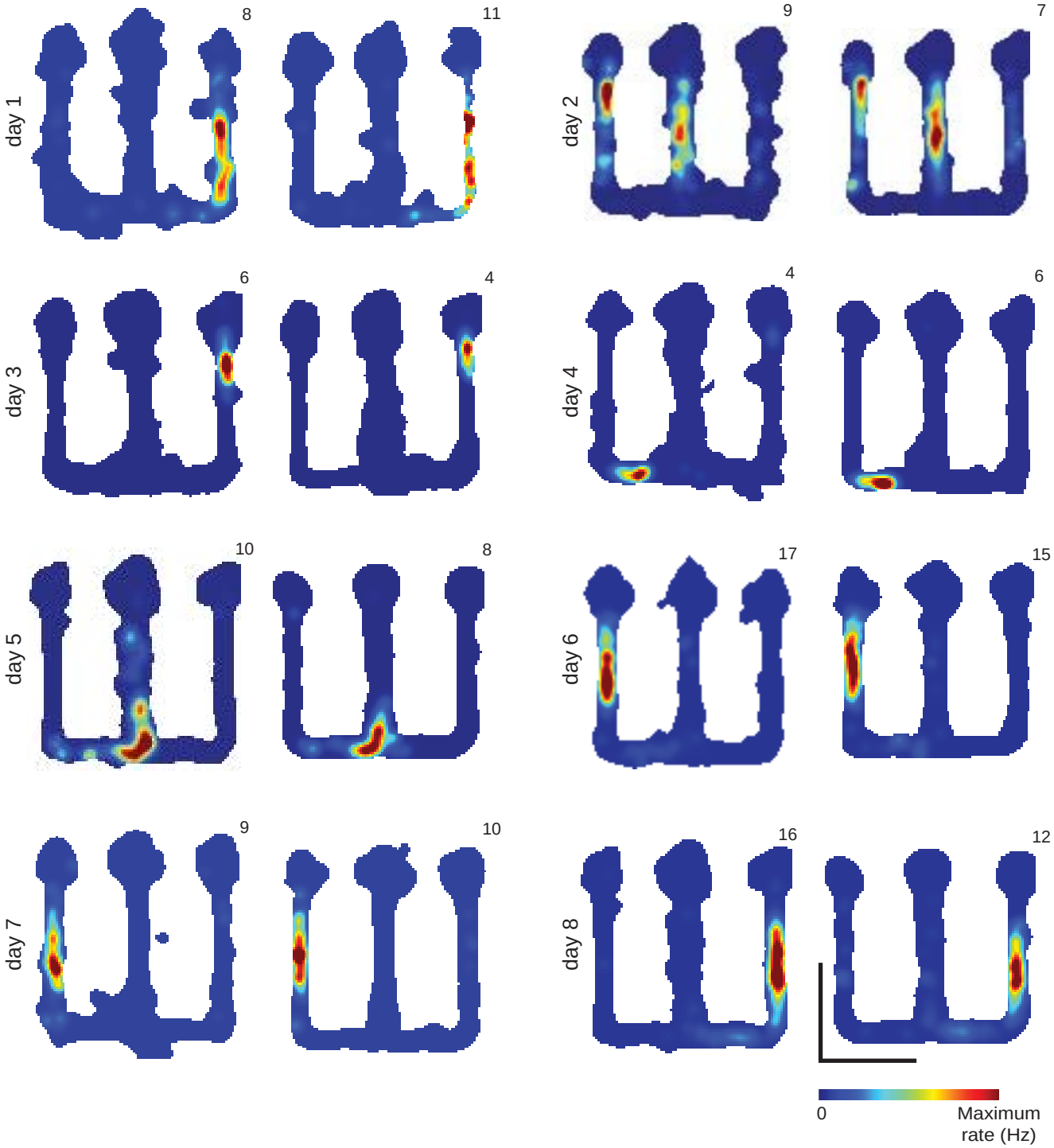

Fig. S10: Place fields. Place fields from SWR disruption animals during the two run sessions from different days. Color plots represent occupancy-normalized firing rates of place cells on the maze. Numbers on top right of each plot denote maximum firing rate of the cell in the two-dimensional map in that particular run session. Note the similarity of the place fields across the run sessions on each day. Scale bars represent 40 cm in each dimension (shown in bottom right panel).

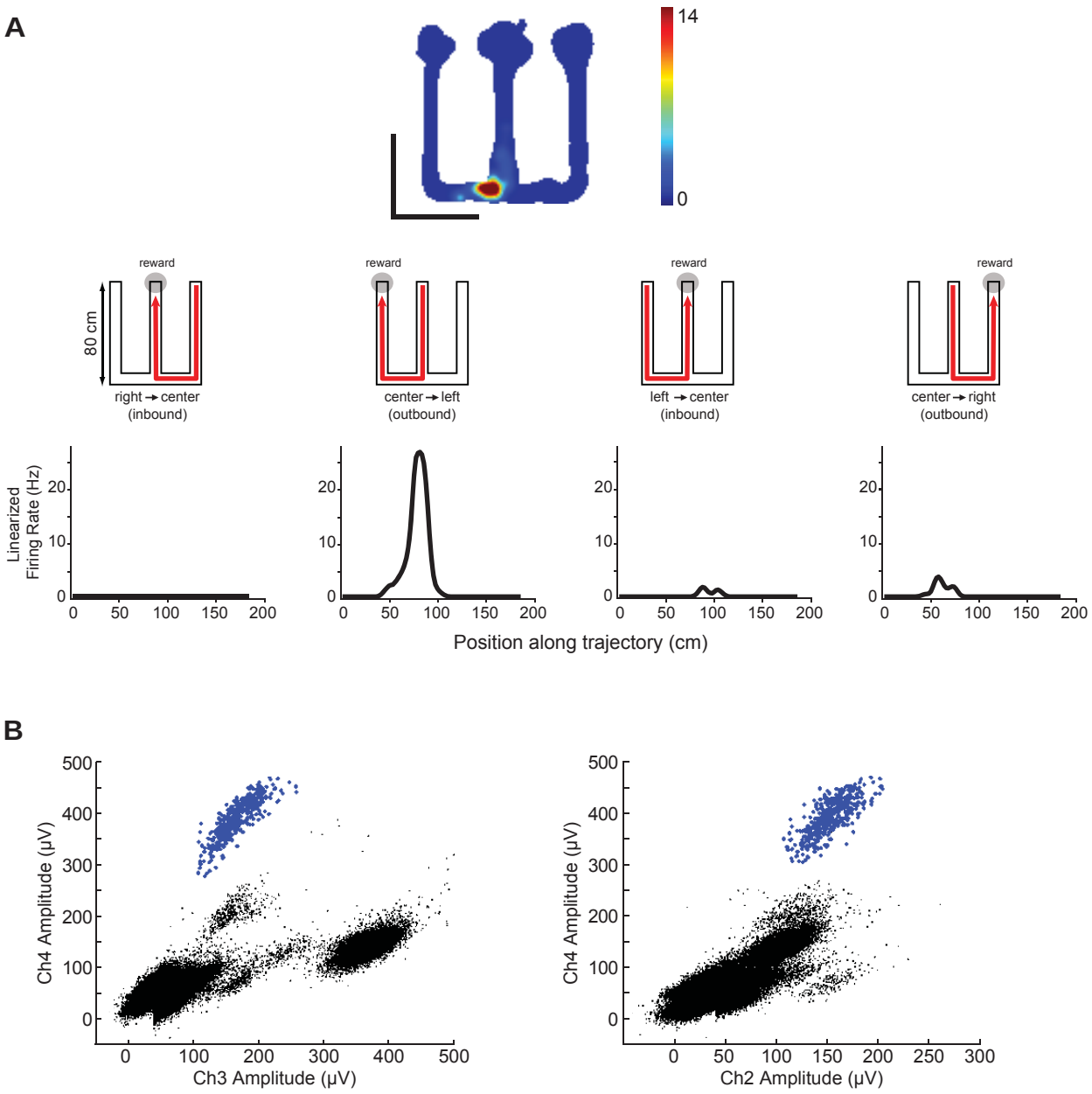

Fig. S11: Linearized place fields. (**A)** Linearized place fields for an example place cell in the SWR disruption group. *(Top)* Two-dimensional occupancy normalized firing rate map of the place cell. Scale bars are 40 cm in each dimension. *(Bottom)* Linearized firing rate for each of the 4 trajectories illustrated in the schematic (similar to Fig. 1A). Linearized place fields were used to calculate peak rate, place field size, stability and overlap of place fields. (**B)** Subset of the cluster plots for the place cell in **A**. Each plot shows the isolated cluster (blue dots) in two amplitude dimensions.

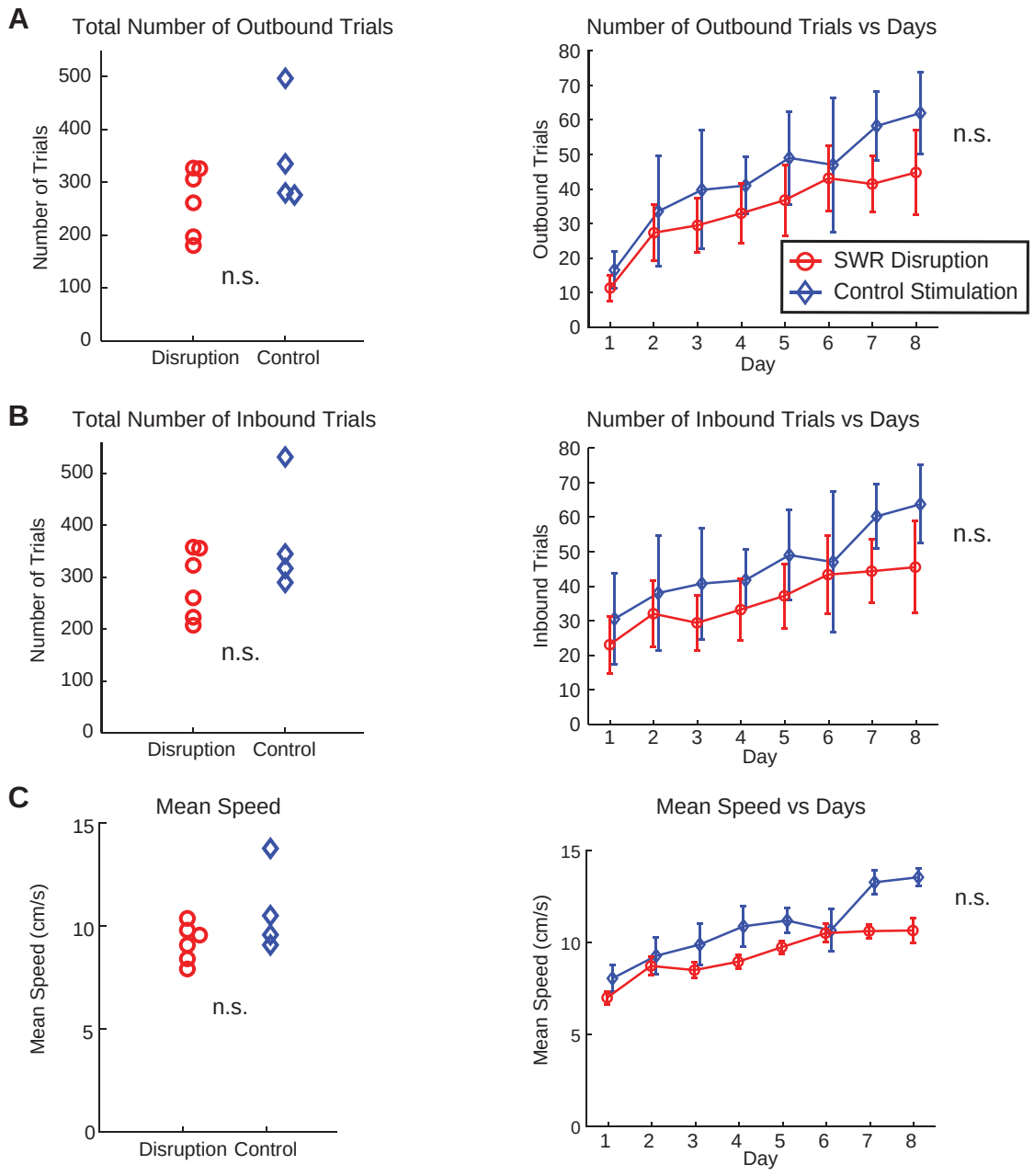

Fig. S12: Behavior parameters. (A) *(Left)* Total number of outbound trials performed by each animal in the SWR disruption and control stimulation group (n = 6, 4; n.s., rank-sum test, p > 0.26). *(Right)* Number of outbound trials vs day number for the SWR disruption and control stimulation group (curves offset for clarity; n = 6, 4; error bars represent s.e.m.; n.s., repeated measures ANOVA, main effect of group, p > 0.22). **(B)** *(Left)* Total number of inbound trials performed by each animal in the SWR disruption and control stimulation group (n = 6, 4; n.s., rank-sum test, p > 0.48). *(Right)* Number of inbound trials vs day number for the SWR disruption and control stimulation group (curves offset for clarity; n = 6, 4; error bars represent s.e.m.; n.s., repeated measures ANOVA, main effect of group, p > 0.24). **(C)** *(Left)* Mean speed for each animal in the SWR disruption and control stimulation group (n = 6, 4; n.s., rank-sum test, p > 0.17). *(Right)* Mean speed vs day number for the SWR disruption and control stimulation group (curves offset for clarity; n = 6, 4; error bars represent s.e.m.; n.s., repeated measures ANOVA, main effect of group, p > 0.15).

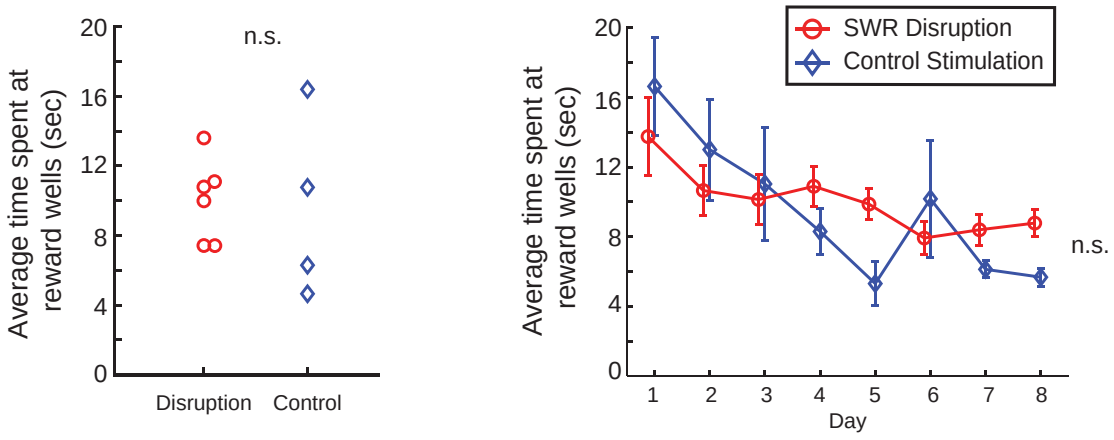

Fig. S13: Behavior parameters - Time spent at reward wells. *(Left)* Average time spent at reward wells between trajectories by each animal in the SWR disruption and control stimulation group (n = 6, 4; n.s., rank-sum test, $p > 0.5$). *(Right)* Average time spent at reward wells vs day number for the SWR disruption and control stimulation group (curves offset for clarity; n = 6, 4 each; error bars represent s.e.m.; n.s., repeated measures ANOVA, main effect of group, $p > 0.5$). Time spent at the individual reward wells (center and side wells) was similar.

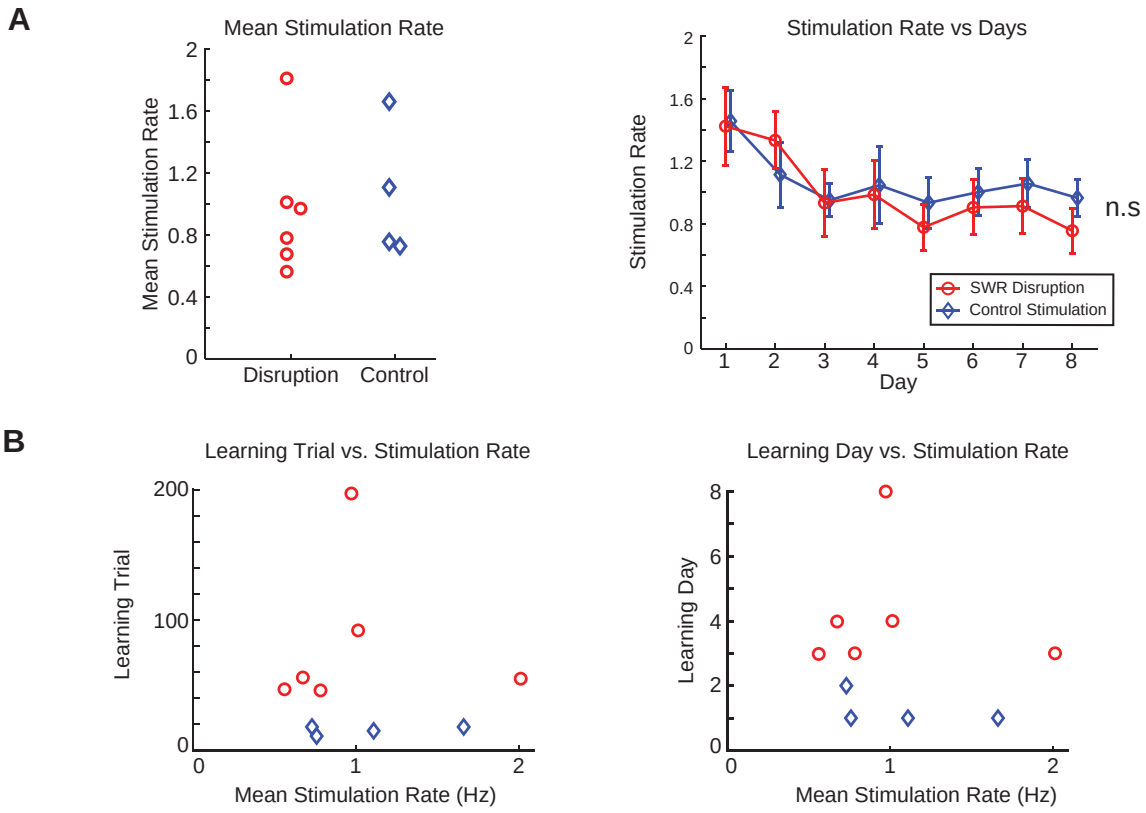

Fig. S14: Stimulation Controls. (A) *(Left)* Mean stimulation rate for each animal in the SWR disruption and control stimulation group (n = 6, 4; n.s., rank-sum test, p > 0.5). *(Right)* Mean stimulation rate vs day number for the SWR disruption and control stimulation group (curves offset for clarity, n = 6, 4, error bars represent s.e.m., n.s., repeated measures ANOVA, main effect of group, p > 0.5). **(B)** Learning rate does not depend upon stimulation rate. Learning trial (*Left*) and learning day (*Right*) plotted as a function of mean stimulation rate for each animal in the SWR disruption and control stimulation groups. None of the correlations are significant (rank correlations, p's > 0.48).

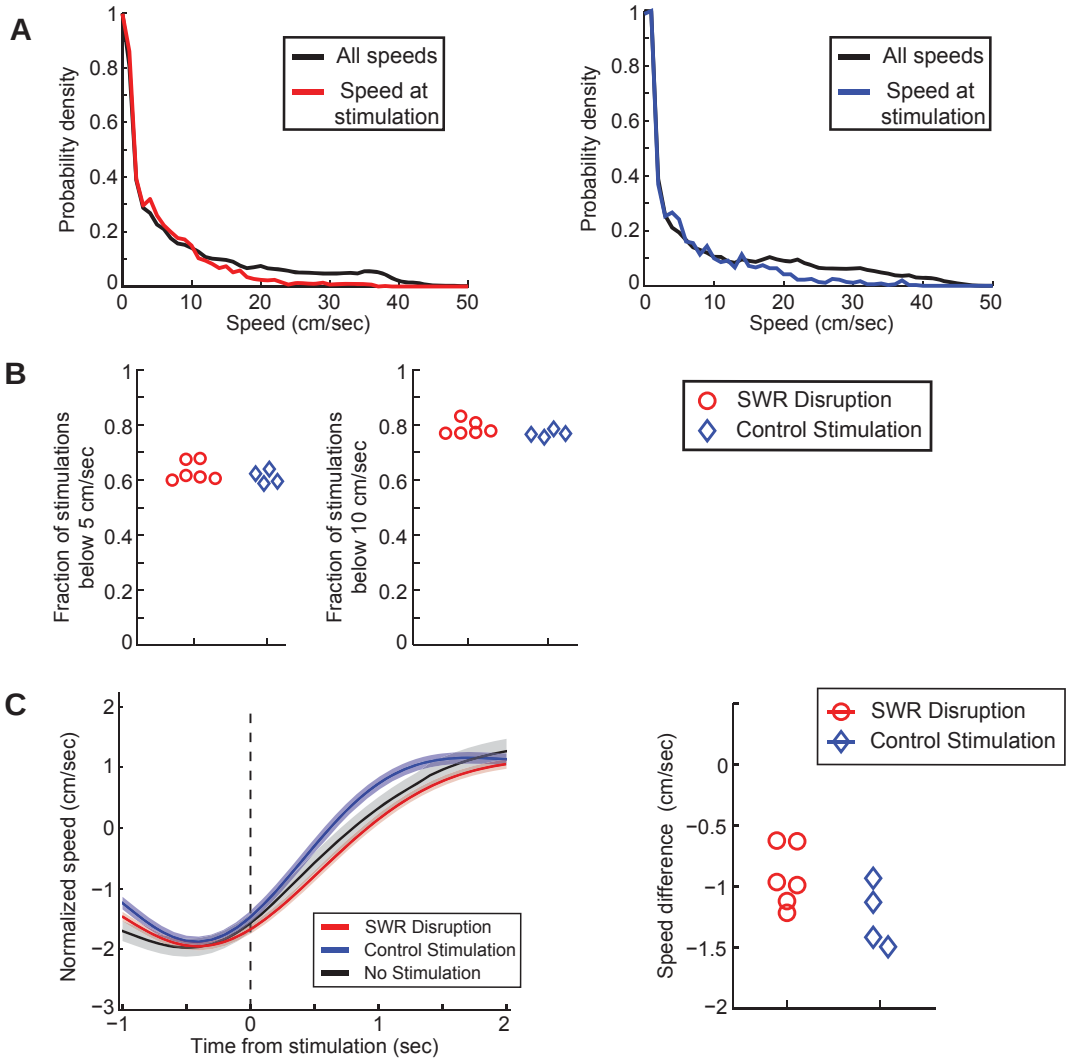

Fig. S15: Stimulation Controls - Speed at stimulation. (A) Speed during stimulation. Single day examples from *(Left)* a SWR disruption animal, and *(Right)* a control stimulation animal, showing normalized distribution of all speeds during behavior and normalized distribution of speeds at which stimulation occurred. (**B)** Fraction of stimulations that occurred when the speed of the animal was < 5 cm/sec and < 10 cm/sec for each animal in the two groups. The proportions are similar for the two groups (n = 6, 4, n.s., rank-sum test, $p > 0.12$). **(C)** No effect of stimulation on running speed. *(Left)* Normalized speed (normalized by subtracting mean speed) in 100 ms bins around the time of stimulation (vertical dotted black line) for SWR disruption (red) and control stimulation (blue) animals. Mean curves and s.e.m. error (shown by shaded area) are derived from all stimulations on all days for all animals in the SWR disruption (n = 86644 events in 48 days) and the control stimulation group (n = 60227 events in 32 days). Normalized speed is also shown for animals with similar detection of online ripples but with no stimulation (black, n = 7608 events in 6 days across 3 animals). All groups show a trend of apparent decrease in speed before the SWR detection event and increase after the detection event, which is due to the fact that SWRs occur preferentially at slow speeds and due to the online speed filter. The actual shape of the curve depends on a complex interaction of these two factors and the animals running behavior. *(Right)* Difference in speed in a 1 second window before and after stimulation for each animal in the SWR disruption and control stimulation groups. The groups are similar (n = 6, 4, n.s., rank-sum test, $p > 0.17$).

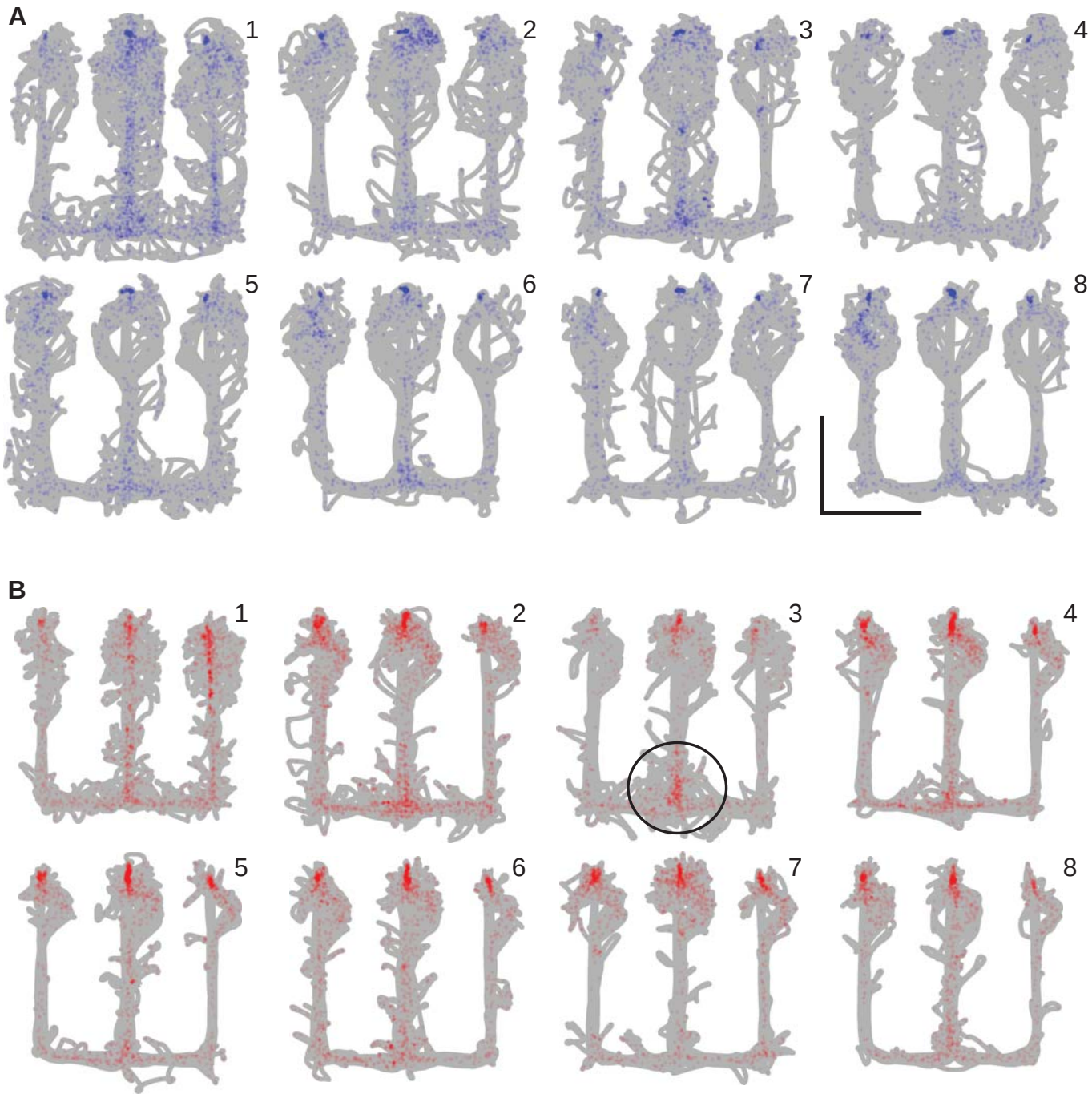

Figure S16: Examples of position during stimulation. (A, B) Position of the animal on the W-maze during stimulation for a representative animal in the control stimulation group (blue markers in **A**) and the SWR disruption group (red markers in **B**). Each panel shows all stimulation locations for a day (day numbers on top right) overlaid on all positions of the animal in that day (gray background). Scale bars (shown in **A**) represent 40 cm in each dimension. Note the concentration of stimulation locations at the reward wells and choice point (illustrated by circle in panel 3 in **B**) in latter days as the track becomes familar.

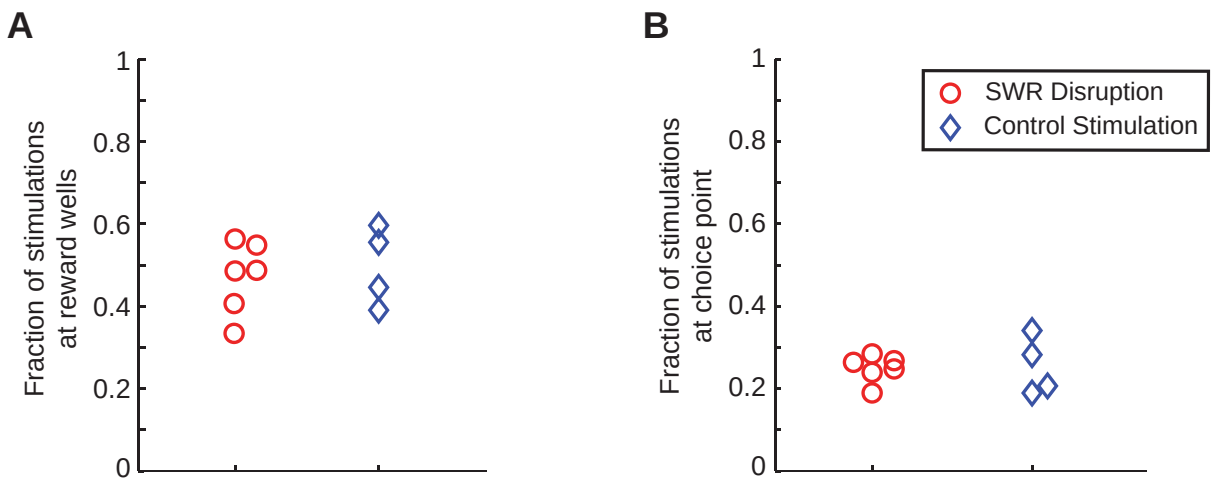

Fig. S17: Stimulation Controls - Position at stimulation. Fraction of stimulations that occurred at **(A)** the reward wells, and **(B)** the choice point, for each animal in the two groups. All stimulations that occurred within a distance of 10 cm from the reward wells and choice point were included. The proportions are similar for the two groups (n = 6, 4, n.s., rank-sum test, $p > 0.5$ for both comparisons).

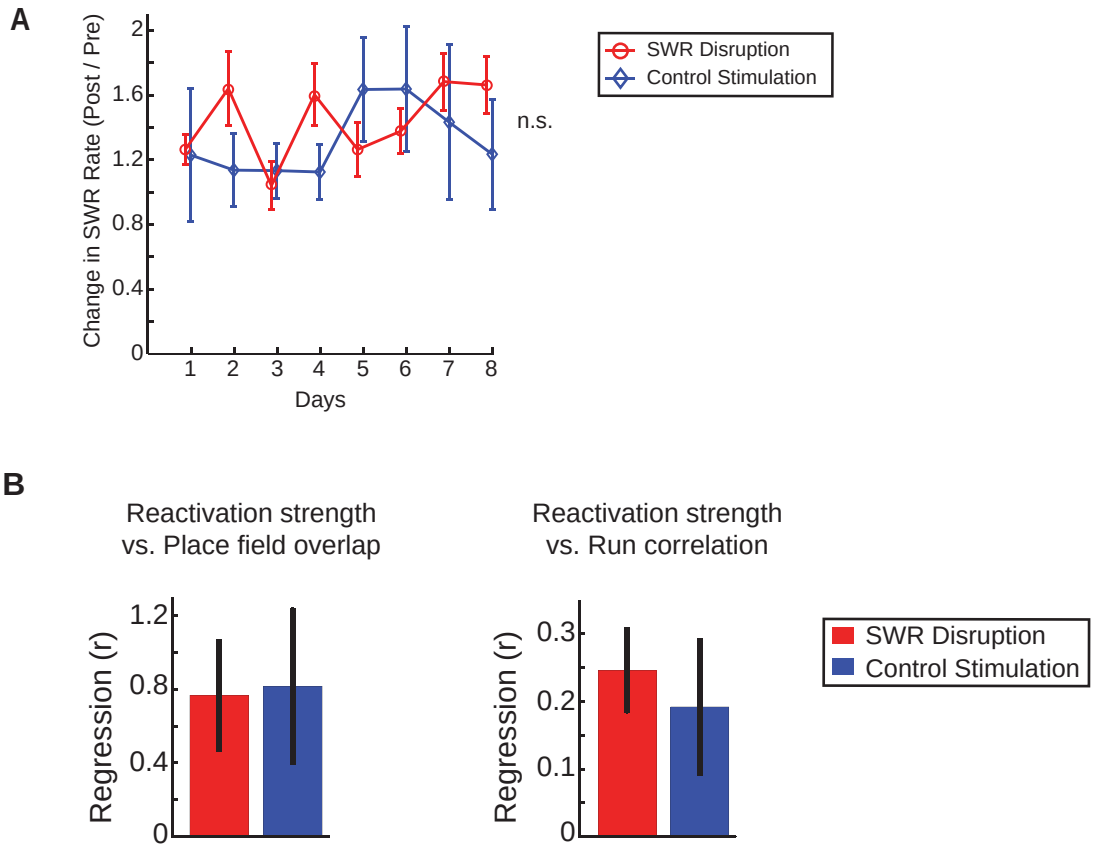

Fig. S18: Reactivation during SWRs in rest periods after behavior. (A) Fraction change in SWR rate during rest (SWR rate in *Post* rest period after behavior / SWR rate in *Pre* rest period before behavior) vs day number for the SWR disruption and control stimulation group (curves offset for clarity, n = 6, 4, error bars represent s.e.m., n.s., $p > 0.28$, repeated measures ANOVA, main effect of group). **(B)** Reactivation during SWRs in rest periods after behavior is seen in both the SWR disruption and control stimulation group. Reactivation strength was defined as the difference in correlated firing during the rest sessions (*Post-Pre*, 100 ms window). *(Left)* Regression between reactivation strength and place field overlap (corresponding to scatter-plot shown in Fig. 4B) for the two groups. Error bars represent 95% confidence intervals. *(Right)* Regression between reactivation strength and run correlations (200 ms window) for the two groups. Both regressions are highly significant ($p < 0.001$). Error bars represent 95% confidence intervals.

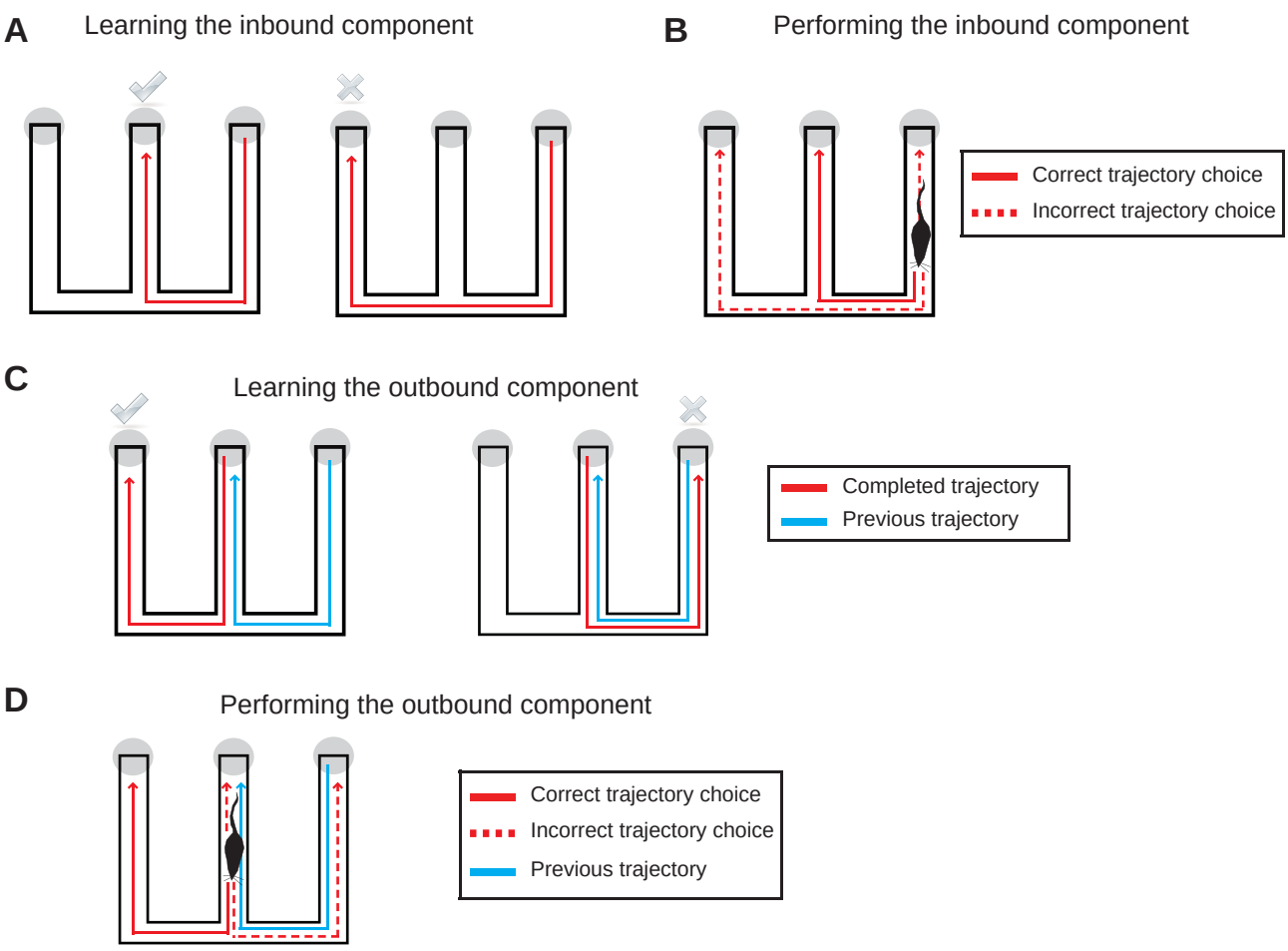

Fig. S19: Requirements for task learning and performance. (A) Learning the inbound rule. Learning the inbound rule. The information necessary to learn the inbound trials is available when animals arrive at a center or outer arm food well from an outer arm. The animals can then learn that reward is only available if they are in the center arm and came from an outer arm. This requires integrating information about immediate past location with the presence or absence of reward. **(B)** Applying the inbound rule. Once the inbound rule is learned, applying the rule requires only that the animals can identify their current location as being in one of the other arms and retrieve the correct association that indicates that they should proceed to the center arm. Thus, performing the inbound task does not require memory for immediate past locations or integration of past and possible future locations. **(C)** Learning the outbound rule. The information required to learn the outbound rule is available when animals arrive at the food well on an outer arm and either receive or do not receive reward. Reward is only available when animals have just come from the center arm and, prior to that, arrived in the center arm from the opposite outer arm. Thus, the animal would likely integrate information about reward with both the more remote memory of the previous inbound trajectory and the immediate past memory for the most recent outbound trajectory. Remote awake replay events that reactivate trajectories from temporally and spatially distant experiences may be critical for this learning. **(D)** Applying the outbound rule. To apply the outbound rule the animal must be able to identify its current location as being in the center arm, remember the immediate past trajectory from one of the outer arms, and use the memory of the past location to plan and execute

a movement to the opposite outer arm. We suggest that the replay of past and possible future trajectories during awake SWRs provides the representational substrate for linking past and future trajectories during decision making. We note here that the replay of possible future trajectories is presumably also a manifestation of memory retrieval, as knowing the future possibilities likely depends on past experience with those possibilities.

Overall, the fact that SWR interruption had no effect on the learning or application of the inbound rule indicates that SWRs are not necessary for the retrieval of memories for immediate past experiences. It therefore seems likely that these experiences are represented in other cortical areas such as the temporal or prefrontal cortex. Awake SWRs would therefore be expected to be most important when more remote memories are needed, as is the case for the learning of the outbound rule or when future possibilities need to be evaluated in the context of specific past experiences, as when the animals apply the outbound rule. Thus, in the absence of awake replay, we would expect that outbound learning would depend on slower learning systems such the basal ganglia which, given sufficient numbers of trials, could perhaps learn a specific set of turns that would take the animal from one outer arm to the center arm and then to the other outer arm (e.g. right, right, turn around, right, right).

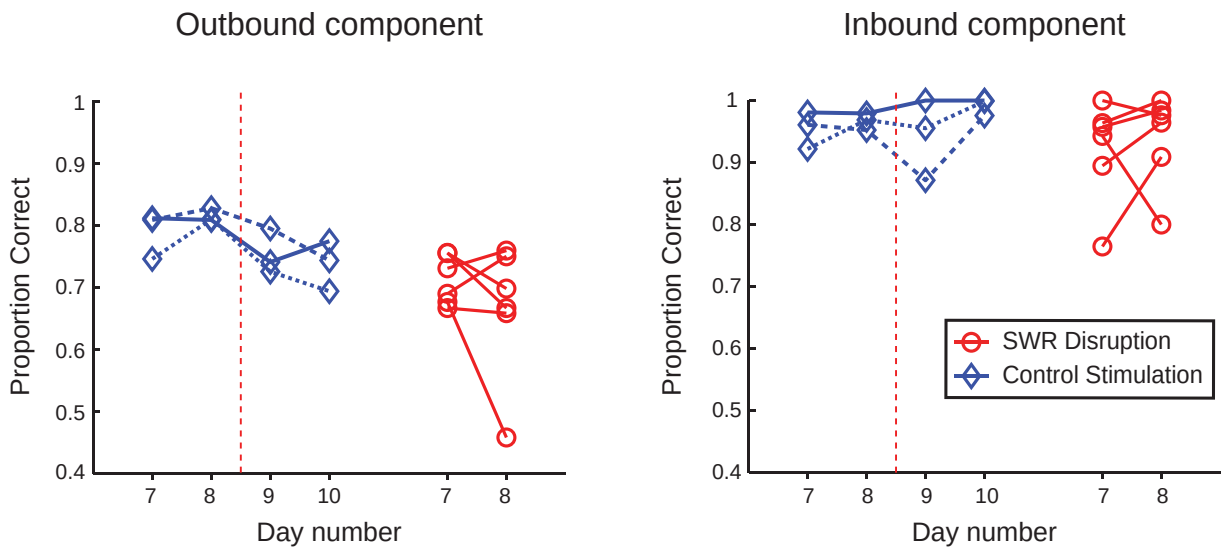

Fig. S20: Effect of SWR disruption on control stimulation animals. Change in average performance for 3 control stimulation animals from days 7-8 (last 2 days of control stimulation) to days 9-10 (switch to SWR disruption) is plotted along with average performance on days 7-8 for SWR disruption animals, for *(Left)* outbound and *(Right)* inbound components. For each control stimulation animal, outbound performance on days 9 and 10 during SWR disruption was worse than the corresponding performance on days 7 and 8. We pooled together data from the 3 control stimulation animals and compared the proportion of correct trials during control stimulation (days 7-8) to those during SWR disruption (days 9-10) using a two-proportion Z-test. For the outbound, working memory component, animals performed 262 correct trials out of a total of 327 total trials performed during control stimulation on days 7 and 8 (proportion of 0.80 correct), which reduced to 229 correct out of a total of 317 total trials performed during SWR disruption on days 9-10 (proportion of 0.72 correct). Under the assumption of independent trials, this corresponds to a Z-value of 2.35 and a corresponding p value of 0.02 ($p < 0.05$). For the inbound component, the corresponding values were 328 correct out of a total of 342 trials (0.96 correct) and 312 correct out of a total of 325 trials (0.96 correct) on days 7-8 and days 9-10 respectively. This corresponded to a Z-value of 0.06 and $p > 0.5$.

References

1. L. R. Squire, Memory and the hippocampus: A synthesis from findings with rats, monkeys, and humans. *Psychol. Rev.* **99**, 195 (1992). doi:10.1037/0033-295X.99.2.195 Medline

2. H. Eichenbaum, N. J. Cohen, *From Conditioning to Conscious Recollection* (Oxford Univ. Press, New York, 2001).

3. G. Riedel *et al*., Reversible neural inactivation reveals hippocampal participation in several memory processes. *Nat. Neurosci.* **2**, 898 (1999). doi:10.1038/13202 Medline

4. D. S. Olton, J. T. Becker, G. E. Handelmann, Hippocampus, space, and memory. *Behav. Brain Sci.* **2**, 313 (1979). doi:10.1017/S0140525X00062713

5. J. O'Keefe, L. Nadel, *The Hippocampus as a Cognitive Map* (Oxford Univ. Press, London, 1978).

6. M. A. Wilson, B. L. McNaughton, Dynamics of the hippocampal ensemble code for space. *Science* **261**, 1055 (1993). doi:10.1126/science.8351520 Medline

7. G. Buzsáki, Hippocampal sharp waves: Their origin and significance. *Brain Res.* **398**, 242 (1986). doi:10.1016/0006-8993(86)91483-6 Medline

8. J. O'Neill, T. Senior, J. Csicsvari, Place-selective firing of CA1 pyramidal cells during sharp wave/ripple network patterns in exploratory behavior. *Neuron* **49**, 143 (2006). doi:10.1016/j.neuron.2005.10.037 Medline

9. D. J. Foster, M. A. Wilson, Reverse replay of behavioural sequences in hippocampal place cells during the awake state. *Nature* **440**, 680 (2006). doi:10.1038/nature04587 Medline

10. K. Diba, G. Buzsáki, Forward and reverse hippocampal place-cell sequences during ripples. *Nat. Neurosci.* **10**, 1241 (2007). doi:10.1038/nn1961 Medline

11. M. P. Karlsson, L. M. Frank, Awake replay of remote experiences in the hippocampus. *Nat. Neurosci.* **12**, 913 (2009). doi:10.1038/nn.2344 Medline

12. T. J. Davidson, F. Kloosterman, M. A. Wilson, Hippocampal replay of extended experience. *Neuron* **63**, 497 (2009). doi:10.1016/j.neuron.2009.07.027 Medline

13. A. S. Gupta, M. A. van der Meer, D. S. Touretzky, A. D. Redish, Hippocampal replay is not a simple function of experience. *Neuron* **65**, 695 (2010). doi:10.1016/j.neuron.2010.01.034 Medline

14. M. A. Wilson, B. L. McNaughton, Reactivation of hippocampal ensemble memories during sleep. *Science* **265**, 676 (1994). doi:10.1126/science.8036517 Medline

15. G. Buzsáki, The hippocampo-neocortical dialogue. *Cereb. Cortex* **6**, 81 (1996). doi:10.1093/cercor/6.2.81 Medline

16. H. S. Kudrimoti, C. A. Barnes, B. L. McNaughton, Reactivation of hippocampal cell assemblies: effects of behavioral state, experience, and EEG dynamics. *J. Neurosci.* **19**, 4090 (1999). Medline

17. G. Girardeau, K. Benchenane, S. I. Wiener, G. Buzsáki, M. B. Zugaro, Selective suppression of hippocampal ripples impairs spatial memory. *Nat. Neurosci.* **12**, 1222 (2009). doi:10.1038/nn.2384 Medline

18. V. Ego-Stengel, M. A. Wilson, Disruption of ripple-associated hippocampal activity during rest impairs spatial learning in the rat. *Hippocampus* **20**, 1 (2010). Medline

19. D. Dupret, J. O'Neill, B. Pleydell-Bouverie, J. Csicsvari, The reorganization and reactivation of hippocampal maps predict spatial memory performance. *Nat. Neurosci.* **13**, 995 (2010). doi:10.1038/nn.2599 Medline

20. J. O'Neill, B. Pleydell-Bouverie, D. Dupret, J. Csicsvari, Play it again: Reactivation of waking experience and memory. *Trends Neurosci.* **33**, 220 (2010). doi:10.1016/j.tins.2010.01.006 Medline

21. M. F. Carr, S. P. Jadhav, L. M. Frank, Hippocampal replay in the awake state: A potential substrate for memory consolidation and retrieval. *Nat. Neurosci.* **14**, 147 (2011). doi:10.1038/nn.2732 Medline

22. A. C. Singer, L. M. Frank, Rewarded outcomes enhance reactivation of experience in the hippocampus. *Neuron* **64**, 910 (2009). doi:10.1016/j.neuron.2009.11.016 Medline

23. S. Cheng, L. M. Frank, New experiences enhance coordinated neural activity in the hippocampus. *Neuron* **57**, 303 (2008). doi:10.1016/j.neuron.2007.11.035 Medline

24. S. M. Kim, L. M. Frank, Hippocampal lesions impair rapid learning of a continuous spatial alternation task. *PLoS ONE* **4**, e5494 (2009). doi:10.1371/journal.pone.0005494 Medline

25. See supplementary materials on *Science* Online.

26. A. C. Smith *et al*., Dynamic analysis of learning in behavioral experiments. *J. Neurosci.* **24**, 447 (2004). doi:10.1523/JNEUROSCI.2908-03.2004 Medline

27. G. Dragoi, K. D. Harris, G. Buzsáki, Place representation within hippocampal networks is modified by long-term potentiation. *Neuron* **39**, 843 (2003). doi:10.1016/S0896-6273(03)00465-3 Medline

28. J. O'Neill, T. J. Senior, K. Allen, J. R. Huxter, J. Csicsvari, Reactivation of experience-dependent cell assembly patterns in the hippocampus. *Nat. Neurosci.* **11**, 209 (2008). doi:10.1038/nn2037 Medline

29. D. Reisel *et al*., Spatial memory dissociations in mice lacking GluR1. *Nat. Neurosci.* **5**, 868 (2002). doi:10.1038/nn910 Medline

30. A. J. Murray *et al*., Parvalbumin-positive CA1 interneurons are required for spatial working but not for reference memory. *Nat. Neurosci.* **14**, 297 (2011). doi:10.1038/nn.2751 Medline

31. C. Ninness *et al*., Small group statistics: A Monte Carlo comparison of parametric and randomization tests. *Behav. Soc. Issues* **12**, 53 (2002).

32. G. B. Drummond, S. L. Vowler, Different tests for a difference: How do we do research? *J. Physiol.* **590**, 235 (2012). Medline

33. M. B. Zugaro, L. Monconduit, G. Buzsáki, Spike phase precession persists after transient intrahippocampal perturbation. *Nat. Neurosci.* **8**, 67 (2005). Medline

34. G. Buzsáki, G. Czéh, Commissural and perforant path interactions in the rat hippocampus. Field potentials and unitary activity. *Exp. Brain Res.* **43**, 429 (1981). Medline

35. G. Buzsáki, Feed-forward inhibition in the hippocampal formation. *Prog. Neurobiol.* **22**, 131 (1984). Medline